Analyzing COVID-19 Data in the Canadian Province of Manitoba: A New Approach

Leila Amiri[a,*], Mahmoud Torabi[a], Rob Deardon[b]

[a] *Departments of Community Health Sciences & Statistics, University of Manitoba, Winnipeg, Manitoba, Canada*

[b] *Department of Mathematics and Statistics & Faculty of Veterinary Medicine, University of Calgary, Calgary, Canada*

Abstract

The basic homogeneous SEIR (susceptible-exposed-infected-removed) model is a commonly used compartmental model for analyzing infectious diseases such as influenza and COVID-19. However, in the homogeneous SEIR model, it is assumed that the population of study is homogeneous and, one cannot incorporate individual-level information (e.g., location of infected people, distance between susceptible and infected individuals, vaccination status) which may be important in predicting new disease cases. Recently, a geographically-dependent individual-level model (GD-ILM) within an SEIR framework was developed for when both regional and individual-level spatial data are available. In this paper, we propose to use an SEIR GD-ILM for each health region of Manitoba (central Canadian province) population to analyze the COVID-19 data. As different health regions of the population under study may act differently, we assume that each health region has its own corresponding parameters determined by a homogeneous SEIR model (such as contact rate, latent period, infectious period). A Monte Carlo Expectation Conditional Maximization (MCECM) algorithm is used for inference. Using estimated parameters we predict the infection rate at each health region of Manitoba over time to identify highly risk local geographical areas. Performance of the proposed approach is also evaluated through simulation studies.

Keywords: Expectation Conditional Maximization algorithm; Geographically-dependent individual level model; Infectious diseases; Susceptible-exposed-infected-removed model.

*Leila Amiri

Email address: leila.amiri@umanitoba.ca (Leila Amiri)

1. Introduction

The unprecedented coronavirus disease COVID-19 first appeared in Wuhan , China in December 2019 and due to its rapid growth across the globe, the World Health Organization declared a global pandemic on March 11, 2020. According to the COVID-19 dashboard provided by the government of Manitoba, Canada (https://www.arcgis.com/apps/dashboards/c7814c9d73e840f6be29c0ae0430c4bf), every health region of Manitoba has been affected differently in terms of incidence and mortality patterns. Modelling the spread of diseases such as COVID-19 is often aided by incorporating spatial-temporal dynamics in the model. Much statistical and epidemiological research has been carried out to analyze the spatial spread of COVID-19 and its association with potential influencing factors including socio-economic (e.g., income, unemployment rate, population mobility, household density), demographic (e.g., age, sex), environmental (e.g., temperature, wind spread), and epidemiological and healthcare-related (e.g., tuberculosis incidence, social distancing, testing facilities) variables. For example, Chen et al. (2020) applied a Bayesian spatio-temporal model for determining the distribution of COVID-19 cases and its correlation with the migration of the Wuhan population in the early stages of the epidemic. de Souza et al. (2020) studied the relationship between COVID-19 incidence, mortality, case fatality rates and living conditions such as income, education, and urban infrastructure. They used bivariate spatial correlation and multivariate and spatial regression models for the analysis of COVID-19 in Brazil. They showed that municipalities with low living standards had high exposure rates and that urgent measures would have been needed to control the spread of disease in such regions. Santos et al. (2020) created choropleth maps of Rio De Janeiro, Brazil via ArcGIS and found that city neighbourhoods with higher rates of seniors in the population (60+ years), higher tuberculosis incidence, and higher average household density, were more vulnerable to COVID-19. Macharia et al. (2020) used ArcGIS zonal statistics and arithmetic means and found that COVID-19 risk was heterogeneously distributed across multiple social epidemiological indicators in Kenya. They demonstrated that, for instance, people living in areas with low socio-economic status and with poor access to sanitation and hand washing facilities were at higher risk of contracting COVID-19. Zhang and Schwartz (2020) used multivariate regression to investigate the spatial pattern of COVID-19 cases in the United States of America (USA). Their study indicated that there is a positive correlation between COVID-19 incidence and mortality rates and socioeconomic factors including population density, proportion of population aged 65+, poverty, and the percentage of the population tested. Xiong et al. (2020) applied spatial autocorrelation and Spearman's rank correlation methods to investigate the association between COVID-19 cases and environmental factors (e.g., land area and range of elevation) and socio-economic factors (e.g., registered population and resident population). Ram'ırez and Lee (2020) used inverse distance weighted interpolation techniques and Pearson's correlation in ArcGIS and demonstrated that poverty and

unemployment in rural areas, and population density and asthma rates in urban areas, were factors associated with higher COVID-19-related mortality in Colorado, USA.

The typical way for modeling spread of infectious disease in communities is to compartmentalize individuals within the population based on their disease status. One commonly used compartmental framework for diseases such as COVID-19 is the susceptible-exposed-infected-removed (SEIR) model which divides the population into four stages of infection: susceptible, exposed, infectious and removed. As it is simplest, an ordinary differential equation (ODE)-based approach can be used, resulting in what is traditionally known as the *SEIR model*, a popular deterministic mathematical model (Anderson and May; 1992). This model allows for a latent period (time during which an individual is infected but not yet infectious). However, the basic model assumes homogeneity in a closed population. It is relatively easy to extend this model to allow for simple population structure (e.g., age stratification). Such models have heavily been utilized to model and predict the transmission dynamics of COVID-19 (e.g., Giordano et al. 2020; Kissler et al. 2020; Tuite et al. 2020; He et al. 2020; Cooper et al. 2020; ben Khedher et al. 2021; Ghostine et al. 2021, and Balsa et al. 2021).

However, COVID-19 is a disease that can be transmitted from human-to-human, and human populations tend to have complex heterogeneous structures. Therefore, using individual-level models which take spatio-temporal dynamics into account should lead to better models of the disease transmission process, and, thus, help policy makers construct more appropriate control strategies to mitigate the severity of the epidemic.
In this paper, we use a geographically-dependent individual level model (GD-ILM), introduced by Mahsin et al. (2020) which is designed to model the transmission between disease states (e.g., SEIR) on the individual-level over time. Mahsin et al. (2020) set GD-ILMs within a Bayesian framework using Markov chain Monte Carlo methods for statistical inference, and applied their approach to influenza data from Calgary, Canada. Amiri et al. (2021) developed a frequentist approach for GD-ILMs, using an expectation conditional maximization (ECM) algorithm, fitting GD-ILMs for the purpose of analyzing the spatial dynamics of tuberculosis in Manitoba, Canada. In both works, an SIR compartmental framework was employed. GD-ILMs are an extension of ILM framework introduced by Deardon et al. (2010). The key feature of GD-ILMs and ILMs is that they allow for covariate information on susceptible, exposed, and infectious individuals (e.g., age, sex, genetics, lifestyle factors) as well as shared covariate information such as spatial distance between individuals or contact measures (e.g., coronavirus for a shared household or workplaces). However, GD-ILMs also allow regional-level spatial effects to be accounted for and modelled, as well as the individual-level effects ILMs account for.

In this paper, we analyze the second wave of COVID-19 across the five health regions of Manitoba province, Canada, from October 1, 2020 to January 31, 2021 using a two stage approach. The initial consideration of the dynamics of COVID-19 transmission are

based on a homogeneous "classical" SEIR model. This analysis reveals that each of the five health regions of Manitoba has different latent and infectious periods (see Table 1), and, thus, fitting a single SEIR model to the COVID-19 data from the entire Manitoba is likely not appropriate. Accounting for the different health region dynamic may allow us to convey more accurate results to policymakers to make their effective decisions for the prevention and control of COVID-19. Thus we consider seperate GD-ILMs for each health region based upon the estimated latent and infectious periods under the SEIR model. We extend previous GD-ILMs to the SEIR framework and incorporate individual-level covariates (symptomatic/asymptomatic, gender and age) and area-level covariate (Socio-economic status, SES). We develop a Monte Carlo Expectation Conditional Maximization (MCECM) algorithm to carry out the inference in a frequentist framework. We then employ our proposed model to predict the average infectivity rate of COVID-19 in each local geographical area (LGA) of Manitoba over time.

The structure of the rest of this article is as follows: Section 2 presents the homogenous SEIR model and results from analysis of the data for each health region. Section 3 describes our GD-ILM framework and formulation. Parameter estimation is detailed in Section 4. Computation of the standard errors of the model parameter estimates is considered in Section 5. We analyze the COVID-19 data in Section 6. We further investigate performance of the proposed model through simulation studies in Section 7. Some concluding remarks are given in Section 8.

2. SEIR model

In the SEIR model, at each point in continuous time $t \in \Re^+$, four state variables are considered, $S'(t)$, $E'(t)$, $I'(t)$ and $R'(t)$. These denote the numbers of susceptible individuals (who do not have the disease but can contract it), exposed individuals (who are infected but cannot yet transmit the disease), infectious individuals (who have the disease and are capable of spreading it) and recovered individuals (who are considered removed from the population due to the recovery, isolation or death), within the population at time t, respectively. Each individual in the population belongs to one, and only one, of the aforementioned compartments at any given time point. The SEIR model equations are given by

$$\begin{aligned}
\frac{dS'(t)}{dt} &= -\beta' I'(t) S'(t) \\
\frac{dE'(t)}{dt} &= \beta' I'(t) S'(t) - \lambda'_E E'(t), \\
\frac{dI'(t)}{dt} &= \lambda'_E E'(t) - \lambda'_I I'(t),
\end{aligned}$$

Table 1: Results of SEIR model fitting for Manitoba and its five health regions over 500 iterations: contact rate (β'), rounded incubation period (λ_E), and rounded infectious period (λ_I).

Regions	β'	λ_E	λ_I
Interlake	0.2561	3	5
Northern	0.2628	1	7
Southern	0.4827	4	5
Prairie	0.2584	9	5
Winnipeg	0.2255	2	6
Manitoba	0.2421	3	6

$$\frac{dR'(t)}{dt} = \lambda'_I I'(t)$$

in which β' is the transmission rate, $\lambda_E = 1/\lambda'_E$ is the latent period, and $\lambda_I = 1/\lambda'_I$ is the infectious period. Also, $N = S'(t) + E'(t) + I'(t) + R'(t)$ is the total population size.

The main objective of this paper is to consider COVID-19 transmission dynamics across Manitoba from October 1, 2020 to January 31, 2021. The number of daily infected and recovered cases and deaths were provided by Manitoba Health. Manitoba is divided into five health regions named Interlake, Northern, Prairie, Southern and Winnipeg. To examine possible heterogeneity in disease dynamics between the health regions, we fit the SEIR model to data from both the whole of Manitoba, but also each health region separately. We estimate the model parameters through maximum likelihood estimation using the Nelder-Mead algorithm. We conduct 500 simulation studies and use the mean square errors ($MSE = \frac{1}{n}\sum_{i=1}^{n}(y_i - \hat{y}_i)^2$) to measure the accuracy of the fitted model in which y_i is the actual number of reported cases and $\hat{y}_i$ is the number of predicted cases. We then find the best fit to the data as the model with a set of parameters which minimizing mean square errors. The results of fitting the SEIR model are shown in Table 1. As we can see from this table, health regions have varying transmission rates, latent periods and infectious periods. These results motivate us to consider the dynamic of transmission of COVID-19 in Manitoba based on health regions instead of the provincial level. Note that, the latent and infectious periods have been rounded to the nearest integers since they are to be used in a discrete time GD-ILM.

3. Geographically-dependent ILMs with SEIR framework

The discrete-time GD-ILM framework was proposed by Mahsin et al. (2020) and developed by Amiri et al. (2021). The GD-ILM can be defined within different compartmental frameworks, and in this study we consider it in the SEIR framework. In the GD-ILM, the

probability of a susceptible individual i being exposed at time t in area (region) z is:

$$P_{izt} = 1 - \exp\Big(- \Omega_S(i,z) \sum_{j \in I(t,z,\xi(z))} \Omega_T(j,z) k(i,j) + \epsilon(i,z,t) \Big),$$

where z represents the area index which varies from 1 to m, $\xi(z)$ is the set of neighbouring areas that are adjacent to area z, and $I(t,z,\xi(z))$ is the set of infectious individuals at time t in the zth location and its neighbouring areas. $\Omega_S(i,z)$ and $\Omega_T(j,z)$ are functions of susceptibility factors for individual i in area z, and transmissibility factors for infectious individual j in area z, respectively. $k(i,j)$ is the infection kernel that represents shared risk factors associated with both susceptible individual i and infectious individual j; $\epsilon(i,z,t)$ is a spark function and allows for "random spark" infections not well-explained by other model components. In these models, depending on the research goal, one can use individual persons, or aggregated units such as postal codes, dissemination areas (which are the smallest standard geographical area defined in Canada with an average population of 400 to 700 people), as the individual units.

Suppose the study area is divided into m regions and there are n individual units within these m regions. Let $\mathbf{X}_i = (X_{i1}, \ldots, X_{ip_1})^\top$ and $\mathbf{X}_z = (X_{z1}, \ldots, X_{zp_2})^\top$ represent the individual and regional level covariate vectors with dimension p_1 and p_2, corresponding to the susceptible individual unit i ($i = 1, \ldots, n$) and region z ($z = 1, \ldots, m$), respectively. These covariates can be incorporated in the susceptibility function. Moreover, let $\mathbf{W}_j = (W_{j1}, \ldots, W_{jp_3})^\top$ denotes vector of individual level covariate with dimension p_3 corresponding to the infected individual unit j which can be incorporated in the transmibility function. Specifically, $\Omega_S(i,z)$ and $\Omega_T(j,z)$ are defined as:

$$\begin{aligned} \Omega_S(i,z) &= N_i \exp(\alpha_{0S} + \mathbf{X}_i^\top \boldsymbol{\beta}_1 + \mathbf{X}_z^\top \boldsymbol{\beta}_2 + u_z), \\ \Omega_T(j,z) &= n_j \exp(\alpha_{0T} + \mathbf{W}_j^\top \boldsymbol{\beta}_3), \end{aligned}$$

where α_{0S} is the susceptibility intercept, N_i is the number of population recorded for susceptible individual unit i, $\boldsymbol{\beta}_1 = (\beta_{11}, \ldots, \beta_{1p_1})^\top$ and $\boldsymbol{\beta}_2 = (\beta_{21}, \ldots, \beta_{2p_2})^\top$ are the vectors of parameters corresponding to $\mathbf{X}_i$ and $\mathbf{X}_z$, respectively; u_z represents spatial random effects that provide a way of accounting for latent geographic variation or unmeasured covariate effects, here via the specification of some spatial structure between regions. Further, n_j is the number of infectious cases for individual unit j at time t in area z, α_{0T} is the transmibility intercept and $\boldsymbol{\beta}_3 = (\beta_{31}, \ldots, \beta_{3p_3})^\top$ is a vector of coefficients associated with $\mathbf{W}_j$.

Here, the GD-ILM that incorporates these covariates is given by:

$$P_{izt} = 1 - \exp\Big(- N_i \exp(\alpha_{0S} + \mathbf{X}_i^\top \boldsymbol{\beta}_1 + \mathbf{X}_z^\top \boldsymbol{\beta}_2 + u_z) \sum_{j \in I(t,z,\xi(z))} n_j \exp(\alpha_{0T} + \mathbf{W}_j^\top \boldsymbol{\beta}_3) d_{ij}^{-\delta} \Big), \quad (1)$$

where the infection kernel is defined as $k(i,j) = d_{ij}^{-\delta}$ which $\delta > 0$ is the spatial decay parameter and d_{ij} is the Euclidean (earth) distance between susceptible individual i and infectious individual j. For this model, the average infectivity rate at time point t in area z is defined as

$$\bar{\eta_z}(t) = n_z^{-1} \sum_{i=1}^{n_z} P_{izt}, \tag{2}$$

where n_z is the number of individuals in region z.

Among many different choices for modelling the random effect $\mathbf{u} = (u_1, \ldots, u_m)^\top$, we use the Leurox method introduced by Leroux et al. (2000) because it assumes that $\mathbf{u}$ are a weighted combination of a spatially independent effects and a strong spatially dependent effects. Within this framework, $\mathbf{u}$ has a multivariate normal distribution with mean $\mathbf{0}$ and a covariance matrix $\mathbf{\Sigma}_u$ where the generalized inverse of $\mathbf{\Sigma}_u$ is defined as $\mathbf{\Sigma}_u^- = \tau^2[(1-\lambda)\mathbf{I}_m + \lambda\mathbf{D}]$, in which $\mathbf{I}_m$ is the identity matrix of dimension m and $\mathbf{D}$ is the intrinsic autoregression matrix which represents the neighbourhood structure of the regions with typical element,

$$d_{zz'} = \begin{cases} g_z, & z = z', \\ -\mathrm{I}\{z \sim z'\}, & z \neq z'. \end{cases}$$

where g_z is the number of neighbours of region z, $z \sim z'$ indicates that regions z and z' are neighbours, and I is the indicator function. Also, τ^2 and $\lambda \in [0,1]$ are precision and spatial dependence, respectively. The two extreme cases of λ (0 and 1) giving rise to the independence model $\mathbf{\Sigma}_u^- = \tau^2\mathbf{I}_m$ and intrinsic autoregression $\mathbf{\Sigma}_u^- = \tau^2\mathbf{D}$ (Besag et al., 1991).

4. Parameter estimation via the MCECM algorithm

The EM algorithm is a general iterative method for determining maximum likelihood estimators (MLEs) in cases where both observed and latent variables are simultaneously present. The method was first introduced by Hartley (1958), and was later generalized by Dempster et al. (1977). The algorithm consists of two basic steps: expectation (E) and maximization (M) which are successively repeated. In the E step, we compute the expectation of the log-likelihood of complete data given the observed data. In the M step, MLEs are updated by maximizing the obtained function in the E step. However, quite often the EM algorithm cannot be directly applied because the maximization (M) step is difficult to carry out. Thus, Meng and Rubin (1993) proposed an extension of the EM, the Expectation Conditional Maximization (ECM) algorithm, which is easy to implement and more broadly applicable than the EM. The key feature of the ECM is to replace the M-step of the EM with several analytically tractable conditional maximization

(CM) steps. Moreover, it shares the appealing features of the EM, while often resulting in faster convergence. Let $\mathbf{y}, \mathbf{z}$ and $\mathbf{u}$ indicate the vectors of responses, corresponding area of each response and spatial random effects, respectively. In this paper, to compute MLEs of $\boldsymbol{\Theta} = (\alpha_{0S}, \alpha_{0T}, \boldsymbol{\beta}_1, \boldsymbol{\beta}_2, \boldsymbol{\beta}_3, \delta, \tau, \lambda)$, based on a random sample $(\mathbf{y}; \mathbf{z}; \mathbf{u})$, we adopt the ECM algorithm as $\mathbf{u}$ is latent. For this purpose, the likelihood function of the complete data, $\mathbf{y}_c = (\mathbf{y}; \mathbf{z}; \mathbf{u})$, is computed as follows:

$$L(\boldsymbol{\Theta}; \mathbf{y}_c) \;\; = \;\; f(\mathbf{u}) f(\mathbf{y}|\mathbf{u}, \mathbf{z}), \tag{3}$$

where $f(\mathbf{u})$ is defined in the Section 3 and the probability mass function $f(\mathbf{y}|\mathbf{u}, \mathbf{z})$ is given by:

$$f(\mathbf{y}|\mathbf{u}, \mathbf{z}) \;\; = \;\; \prod_{t=1}^{T} \left\{ \prod_{i \in S(t,z)} \prod_{z=1}^{m} \Big(1 - P_{izt}\Big)^{I(Z_{it}=z)} \prod_{i \in E(t,z,\xi(z)) \setminus E(t-1,z,\xi(z))} \prod_{z=1}^{m} \Big(P_{izt}\Big)^{I(Z_{it}=z)} \right\},$$

where $S(t, z)$ iis the set of all susceptible individuals at time t in region z, $E(t, z, \xi(z)) \setminus E(t-1, z, \xi(z))$ is the set of all newly exposed individuals at time t in region z and its neighbouring areas, and $I(Z_{it} = z)$ is an indicator function such that for $i = 1, \ldots, n$, $t = 1, \ldots, T$, and $z = 1, \ldots, m$,

$$I(Z_{it} = z) = \begin{cases} 1, & \text{if the } i^{th} \text{ individual at time } t \text{ is in } z^{th} \text{ region,} \\ 0, & \text{otherwise.} \end{cases}$$

4.1. E-step via the Metropolis-Hastings sampler

Let $\mathbf{y}_o = (\mathbf{y}; \mathbf{z})$ denote the observed variables. At the kth iteration of the ECM algorithm with current parameter estimates $\boldsymbol{\Theta}^{(k)}$, $\boldsymbol{\Theta}^{(k+1)}$ is obtained by maximizing $\mathrm{E}\Big[\log L(\boldsymbol{\Theta}; \mathbf{y}_c)|\mathbf{y}_o, \Theta^{(k)}\Big]$ with respect to $\boldsymbol{\Theta}$. The expectation $\mathrm{E}\Big[\log L(\boldsymbol{\Theta}; \mathbf{y}_c)|\mathbf{y}_o, \boldsymbol{\Theta}^{(k)}\Big]$ is taken with respect to $f(\mathbf{u}|\mathbf{y}_o, \boldsymbol{\Theta})$. So, to calculate it we need $f(\mathbf{u}, \mathbf{y}_o|\boldsymbol{\Theta})$ and $f(\mathbf{y}_o|\boldsymbol{\Theta})$. Since direct calculation of $f(\mathbf{y}_o|\boldsymbol{\Theta})$ is not possible for the models considered here, we approximate the expectation using the Monte Carlo EM (MCEM) algorithm proposed by Wei and Tanner (1990). Additionally, we replace the M step in the MCEM algorithm by CM steps leading to an MCECM algorithm. The MCECM algorithm consists of the following steps:

Step 1: Select an initial value $\boldsymbol{\Theta}^{(0)}$ for the ECM sequence,
Step 2: In the $(k+1)^{th}$ iteration of the ECM algorithm, random samples $\Big\{\mathbf{u}_{k+1,1}, \mathbf{u}_{k+1,2}, \ldots, \mathbf{u}_{k+1,L}\Big\}$ are generated from $f(\mathbf{u}|\mathbf{y}_o; \boldsymbol{\Theta}^{(k)})$ via the Metropolis-Hastings algorithm as follows.

Firstly, we let $f(\mathbf{u})$ be the candidate density and $f(\mathbf{u}|\mathbf{y}_o)$ the target density where

$$f(\mathbf{u}|\mathbf{y}_o) \propto f(\mathbf{y}|\mathbf{u},\mathbf{z})f(\mathbf{u}).$$

Then, at the l^{th} $(l = 1,\ldots,L)$ iteration of the Metropolis-Hastings algorithm with current values $\mathbf{u}_{k+1,l}$, we generate a $\mathbf{u}_{new}$ from $f(\mathbf{u})$. Additionally, a value r is generated from a Uniform(0,1) distribution, to be compared with the acceptance probability $\rho = \frac{f(\mathbf{y}|\mathbf{u}_{new})}{f(\mathbf{y}|\mathbf{u}_{k+1,l})}$. Specifically, $\mathbf{u}_{k+1,l+1} = \mathbf{u}_{new}$ if $r \leq \rho$ and $\mathbf{u}_{k+1,l+1} = \mathbf{u}_{k+1,l}$ otherwise.

Step 3: $\mathrm{E}\Big[\log L(\boldsymbol{\Theta};\mathbf{y}_c)|\mathbf{y}_o,\boldsymbol{\Theta}\Big]$ is approximated as

$$\mathrm{E}\Big[\log L(\boldsymbol{\Theta};\mathbf{y}_c)|\mathbf{y}_o,\boldsymbol{\Theta}\Big] = \frac{1}{L}\sum_{l=1}^{L}\log L(\boldsymbol{\Theta};\mathbf{y};\mathbf{u}_{k+1,l}) \tag{4}$$

and then $\boldsymbol{\Theta}^{(k+1)}$ can be obtained by maximizing (4) with respect to (w.r.t.) $\boldsymbol{\Theta}$.
The details of maximization are provided below, and for simplicity, $\mathbf{u}_{k+1,l}$ is indicated by $\mathbf{u}_l$.

4.2. M-step

According to (4), we have

$$\begin{aligned}
&\mathrm{E}\Big[\log L(\boldsymbol{\Theta};\mathbf{y}_c)|\mathbf{y}_o,\boldsymbol{\Theta}\Big] = \sum_{t=1}^{T}\sum_{i\in S(t,z)}\sum_{z=1}^{m} I(Z_{it}=z)\\
&\frac{1}{L}\sum_{l=1}^{L}\left[-N_i\exp\left(\alpha_{0S}+\mathbf{X}_i^\top\boldsymbol{\beta}_1+\mathbf{X}_z^\top\boldsymbol{\beta}_2+u_{zl}\right)\sum_{j\in I(t,z,\xi(z))} n_j\exp(\alpha_{0T}+\mathbf{W}_j^\top\boldsymbol{\beta}_3)d_{ij}^{-\delta}\middle|\mathbf{y}_o\right]\\
&+\sum_{t=1}^{T}\sum_{i\in E(t,z,\xi(z))\setminus E(t-1,z,\xi(z))}\sum_{z=1}^{m} I(Z_{it}=z)\\
&\frac{1}{L}\sum_{l=1}^{L}\left[\ln\left(1-\exp\Big(-N_i\exp(\alpha_{0S}+\mathbf{X}_i^\top\boldsymbol{\beta}_1+\mathbf{X}_z^\top\boldsymbol{\beta}_2+u_{zl})\sum_{j\in I(t,z,\xi(z))} n_j\exp(\alpha_{0T}+\mathbf{W}_j^\top\boldsymbol{\beta}_3)d_{ij}^{-\delta}\Big)\right)\middle|\mathbf{y}_o\right]\\
&-\frac{m}{2}\ln(2\pi)+\frac{m}{2}\ln(\tau^2)+\frac{1}{2}\ln\Big(\big|\lambda\mathbf{D}+(1-\lambda)\mathbf{I}\big|\Big)-\frac{\tau^2}{2}\frac{1}{L}\sum_{l=1}^{L}\left[\mathbf{u}_l^\top\Big(\lambda\mathbf{D}+(1-\lambda)\mathbf{I}\Big)\mathbf{u}_l\middle|\mathbf{y}_o\right].
\end{aligned} \tag{5}$$

We then need to maximize (5) with respect to model parameters.

4.2.1. CM-step 1

α_{0S} is solution of the following equation

$$\frac{\partial\mathrm{E}\Big[\log L(\boldsymbol{\Theta};\mathbf{y}_c)|\mathbf{y}_o,\boldsymbol{\Theta}\Big]}{\partial\alpha_{0S}} = -\sum_{t=1}^{T}\sum_{i\in S(t,z)}\sum_{z=1}^{m} I(Z_{it}=z)N_i\exp(\alpha_{0S}^{(k)}+\mathbf{X}_i^\top\boldsymbol{\beta}_1^{(k)}+\mathbf{X}_z^\top\boldsymbol{\beta}_2^{(k)})$$

$$\sum_{j\in I(t,z,\xi(z))} n_j \exp(\alpha_{0T}^{(k)} + \mathbf{W}_j^\top \boldsymbol{\beta}_3^{(k)}) d_{ij}^{-\delta^{(k)}} \frac{1}{L}\sum_{l=1}^{L}\left[\exp(u_{zl})\middle|\mathbf{y}_o, \boldsymbol{\Theta}^{(k)}\right]$$
$$+\sum_{t=1}^{T}\sum_{i\in E(t,z,\xi(z))\setminus E(t-1,z,\xi(z))}\sum_{z=1}^{m} I(Z_{it}=z) N_i \exp(\alpha_{0S}^{(k)} + \mathbf{X}_i^\top \boldsymbol{\beta}_1^{(k)} + \mathbf{X}_z^\top \boldsymbol{\beta}_2^{(k)})$$
$$\sum_{j\in I(t,z,\xi(z))} n_j \exp(\alpha_{0T}^{(k)} + \mathbf{W}_j^\top \boldsymbol{\beta}_3^{(k)}) d_{ij}^{-\delta^{(k)}} \frac{1}{L}\sum_{l=1}^{L}\left[\frac{(1-P_{izt})}{P_{izt}}\exp(u_{zl})\middle|\mathbf{y}_o, \boldsymbol{\Theta}^{(k)}\right]. \tag{6}$$

Unfortunately, there is no closed-form solution for equation (6). Thus, we employ the Newton-Raphson method to compute the solution to (6). In this regard, we have

$$\frac{\partial^2 \mathrm{E}\Big[\log L(\boldsymbol{\Theta};\mathbf{y}_c)|\mathbf{y}_o,\boldsymbol{\Theta}\Big]}{\partial \alpha_{0S}^2} = -\sum_{t=1}^{T}\sum_{i\in S(t,z)}\sum_{z=1}^{m} I(Z_{it}=z) N_i \exp(\alpha_{0S}^{(k)} + \mathbf{X}_i^\top \boldsymbol{\beta}_1^{(k)} + \mathbf{X}_z^\top \boldsymbol{\beta}_2^{(k)})$$
$$\sum_{j\in I(t,z,\xi(z))} n_j \exp(\alpha_{0T}^{(k)} + \mathbf{W}_j^\top \boldsymbol{\beta}_3^{(k)}) d_{ij}^{-\delta^{(k)}} \frac{1}{L}\sum_{l=1}^{L}\left[\exp(u_{zl})\middle|\mathbf{y}_o, \boldsymbol{\Theta}^{(k)}\right]$$
$$+\sum_{t=1}^{T}\sum_{i\in E(t,z,\xi(z))\setminus E(t-1,z,\xi(z))}\sum_{z=1}^{m} I(Z_{it}=z)\Bigg\{ N_i \exp(\alpha_{0S}^{(k)} + \mathbf{X}_i^\top \boldsymbol{\beta}_1^{(k)} + \mathbf{X}_z^\top \boldsymbol{\beta}_2^{(k)})$$
$$\sum_{j\in I(t,z,\xi(z))} n_j \exp(\alpha_{0T}^{(k)} + \mathbf{W}_j^\top \boldsymbol{\beta}_3^{(k)}) d_{ij}^{-\delta^{(k)}} \frac{1}{L}\sum_{l=1}^{L}\left[\frac{(1-P_{izt})}{P_{izt}}\exp(u_{zl})\middle|\mathbf{y}_o, \boldsymbol{\Theta}^{(k)}\right]$$
$$-N_i^2 \exp(2\alpha_{0S}^{(k)} + 2\mathbf{X}_i^\top \boldsymbol{\beta}_1^{(k)} + 2\mathbf{X}_z^\top \boldsymbol{\beta}_2^{(k)})\Big(\sum_{j\in I(t,z,\xi(z))} n_j \exp(\alpha_{0T}^{(k)} + \mathbf{W}_j^\top \boldsymbol{\beta}_3^{(k)}) d_{ij}^{-\delta^{(k)}}\Big)^2$$
$$\frac{1}{L}\sum_{l=1}^{L}\left[\frac{(1-P_{izt})}{P_{izt}^2}\exp(2u_{zl})\middle|\mathbf{y}_o, \boldsymbol{\Theta}^{(k)}\right]\Bigg\}.$$

The following recursive relationship (first-order Taylor expansion) is obtained for computing α_{0S}:

$$\alpha_{0S}^{(k+1)} = \alpha_{0S}^{(k)} - \frac{\frac{\partial}{\partial \alpha_{0S}}\mathrm{E}\Big[\log L(\boldsymbol{\Theta};\mathbf{y}_c)|\mathbf{y}_o,\boldsymbol{\Theta}^{(k)}\Big]}{\frac{\partial^2}{\partial \alpha_{0S}^2}\mathrm{E}\Big[\log L(\boldsymbol{\Theta};\mathbf{y}_c)|\mathbf{y}_o,\boldsymbol{\Theta}^{(k)}\Big]}.$$

4.2.2. CM-step 2

Let $\alpha_{0S} = \alpha_{0S}^{(k+1)}$. Analogous to the previous estimation, to estimate $\boldsymbol{\beta}_1$, we observe

$$\frac{\partial \mathrm{E}\Big[\log L(\boldsymbol{\Theta};\mathbf{y}_c)|\mathbf{y}_o,\boldsymbol{\Theta}\Big]}{\partial \boldsymbol{\beta}_1} = -\sum_{t=1}^{T}\sum_{i\in S(t,z)}\sum_{z=1}^{m} I(Z_{it}=z) N_i \mathbf{X}_i \exp(\alpha_{0S}^{(k+1)} + \mathbf{X}_i^\top \boldsymbol{\beta}_1^{(k)} + \mathbf{X}_z^\top \boldsymbol{\beta}_2^{(k)})$$

$$\sum_{j\in I(t,z,\xi(z))} n_j \exp(\alpha_{0T}^{(k)} + \mathbf{W}_j^\top \boldsymbol{\beta}_3^{(k)}) d_{ij}^{-\delta^{(k)}} \frac{1}{L}\sum_{l=1}^{L}\left[\exp(u_{zl})\middle|\mathbf{y}_o, \boldsymbol{\Theta}^{(k)}\right]$$
$$+\sum_{t=1}^{T}\sum_{i\in E(t,z,\xi(z))\setminus E(t-1,z,\xi(z))}\sum_{z=1}^{m} I(Z_{it}=z) N_i \mathbf{X}_i \exp(\alpha_{0S}^{(k+1)} + \mathbf{X}_i^\top \boldsymbol{\beta}_1^{(k)} + \mathbf{X}_z^\top \boldsymbol{\beta}_2^{(k)})$$
$$\sum_{j\in I(t,z,\xi(z))} n_j \exp(\alpha_{0T}^{(k)} + \mathbf{W}_j^\top \boldsymbol{\beta}_3^{(k)}) d_{ij}^{-\delta^{(k)}} \frac{1}{L}\sum_{l=1}^{L}\left[\frac{(1-P_{izt})}{P_{izt}}\exp(u_{zl})\middle|\mathbf{y}_o, \boldsymbol{\Theta}^{(k)}\right],$$

and

$$\frac{\partial^2 \mathrm{E}\Big[\log L(\boldsymbol{\Theta};\mathbf{y}_c)|\mathbf{y}_o,\boldsymbol{\Theta}\Big]}{\partial\boldsymbol{\beta}_1\partial\boldsymbol{\beta}_1^\top} = -\sum_{t=1}^{T}\sum_{i\in S(t,z)}\sum_{z=1}^{m} I(Z_{it}=z) N_i \mathbf{X}_i\mathbf{X}_i^\top \exp(\alpha_{0S}^{(k+1)} + \mathbf{X}_i^\top \boldsymbol{\beta}_1^{(k)} + \mathbf{X}_z^\top \boldsymbol{\beta}_2^{(k)})$$
$$\sum_{j\in I(t,z,\xi(z))} n_j \exp(\alpha_{0T}^{(k)} + \mathbf{W}_j^\top \boldsymbol{\beta}_3^{(k)}) d_{ij}^{-\delta^{(k)}} \frac{1}{L}\sum_{l=1}^{L}\left[\exp(u_{zl})\middle|\mathbf{y}_o, \boldsymbol{\Theta}^{(k)}\right]$$
$$+\sum_{t=1}^{T}\sum_{i\in E(t,z,\xi(z))\setminus E(t-1,z,\xi(z))}\sum_{z=1}^{m} I(Z_{it}=z)\Bigg\{ N_i \mathbf{X}_i\mathbf{X}_i^\top \exp(\alpha_{0S}^{(k+1)} + \mathbf{X}_i^\top \boldsymbol{\beta}_1^{(k)} + \mathbf{X}_z^\top \boldsymbol{\beta}_2^{(k)})$$
$$\sum_{j\in I(t,z,\xi(z))} n_j \exp(\alpha_{0T}^{(k)} + \mathbf{W}_j^\top \boldsymbol{\beta}_3^{(k)}) d_{ij}^{-\delta^{(k)}} \frac{1}{L}\sum_{l=1}^{L}\left[\frac{(1-P_{izt})}{P_{izt}}\exp(u_{zl})\middle|\mathbf{y}_o, \boldsymbol{\Theta}^{(k)}\right]$$
$$-N_i^2 \mathbf{X}_i\mathbf{X}_i^\top \exp(2\alpha_{0S}^{(k+1)} + 2\mathbf{X}_i^\top \boldsymbol{\beta}_1^{(k)} + 2\mathbf{X}_z^\top \boldsymbol{\beta}_2^{(k)})\Big(\sum_{j\in I(t,z,\xi(z))} n_j \exp(\alpha_{0T}^{(k)} + \mathbf{W}_j^\top \boldsymbol{\beta}_3^{(k)}) d_{ij}^{-\delta^{(k)}}\Big)^2$$
$$\frac{1}{L}\sum_{l=1}^{L}\left[\frac{(1-P_{izt})}{P_{izt}^2}\exp(2u_{zl})\middle|\mathbf{y}_o, \boldsymbol{\Theta}^{(k)}\right]\Bigg\}.$$

The following recursive equation is used for obtaining $\boldsymbol{\beta}_1$:

$$\boldsymbol{\beta}_1^{(k+1)} = \boldsymbol{\beta}_1^{(k)} - \frac{\frac{\partial}{\partial\boldsymbol{\beta}_1}\mathrm{E}\Big[\log L(\boldsymbol{\Theta};\mathbf{y}_c)|\mathbf{y}_o,\boldsymbol{\Theta}^{(k)}\Big]}{\frac{\partial^2}{\partial\boldsymbol{\beta}_1\partial\boldsymbol{\beta}_1^\top}\mathrm{E}\Big[\log L(\boldsymbol{\Theta};\mathbf{y}_c)|\mathbf{y}_o,\boldsymbol{\Theta}^{(k)}\Big]}.$$

4.2.3. CM-step 3

Let $\alpha_{0S} = \alpha_{0S}^{(k+1)}$ and $\boldsymbol{\beta}_1 = \boldsymbol{\beta}_1^{(k+1)}$. We update $\boldsymbol{\beta}_2^{(k)}$ by maximizing (5) over $\boldsymbol{\beta}_2$, which gives

$$\frac{\partial \mathrm{E}\Big[\log L(\boldsymbol{\Theta};\mathbf{y}_c)|\mathbf{y}_o,\boldsymbol{\Theta}\Big]}{\partial\boldsymbol{\beta}_2} = -\sum_{t=1}^{T}\sum_{i\in S(t,z)}\sum_{z=1}^{m} I(Z_{it}=z) N_i \mathbf{X}_z \exp(\alpha_{0S}^{(k+1)} + \mathbf{X}_i^\top \boldsymbol{\beta}_1^{(k+1)} + \mathbf{X}_z^\top \boldsymbol{\beta}_2^{(k)})$$

$$\sum_{j\in I(t,z,\xi(z))} n_j \exp(\alpha_{0T}^{(k)} + \mathbf{W}_j^\top \boldsymbol{\beta}_3^{(k)}) d_{ij}^{-\delta^{(k)}} \frac{1}{L}\sum_{l=1}^{L}\left[\exp(u_{zl})\middle|\mathbf{y}_o, \boldsymbol{\Theta}^{(k)}\right]$$
$$+\sum_{t=1}^{T}\sum_{i\in E(t,z,\xi(z))\setminus E(t-1,z,\xi(z))}\sum_{z=1}^{m} I(Z_{it}=z) N_i \mathbf{X}_z \exp(\alpha_{0S}^{(k+1)} + \mathbf{X}_i^\top \boldsymbol{\beta}_1^{(k+1)} + \mathbf{X}_z^\top \boldsymbol{\beta}_2^{(k)})$$
$$\sum_{j\in I(t,z,\xi(z))} n_j \exp(\alpha_{0T}^{(k)} + \mathbf{W}_j^\top \boldsymbol{\beta}_3^{(k)}) d_{ij}^{-\delta^{(k)}} \frac{1}{L}\sum_{l=1}^{L}\left[\frac{(1-P_{izt})}{P_{izt}}\exp(u_{zl})\middle|\mathbf{y}_o, \boldsymbol{\Theta}^{(k)}\right],$$

and

$$\frac{\partial^2 \mathrm{E}\Big[\log L(\boldsymbol{\Theta};\mathbf{y}_c)|\mathbf{y}_o,\boldsymbol{\Theta}\Big]}{\partial\boldsymbol{\beta}_2\partial\boldsymbol{\beta}_2^\top} = -\sum_{t=1}^{T}\sum_{i\in S(t,z)}\sum_{z=1}^{m} I(Z_{it}=z) N_i \mathbf{X}_z\mathbf{X}_z^\top \exp(\alpha_{0S}^{(k+1)} + \mathbf{X}_i^\top \boldsymbol{\beta}_1^{(k+1)} + \mathbf{X}_z^\top \boldsymbol{\beta}_2^{(k)})$$
$$\sum_{j\in I(t,z,\xi(z))} n_j \exp(\alpha_{0T}^{(k)} + \mathbf{W}_j^\top \boldsymbol{\beta}_3^{(k)}) d_{ij}^{-\delta^{(k)}} \frac{1}{L}\sum_{l=1}^{L}\left[\exp(u_{zl})\middle|\mathbf{y}_o, \boldsymbol{\Theta}^{(k)}\right]$$
$$+\sum_{t=1}^{T}\sum_{i\in E(t,z,\xi(z))\setminus E(t-1,z,\xi(z))}\sum_{z=1}^{m} I(Z_{it}=z)\Bigg\{ N_i \mathbf{X}_z\mathbf{X}_z^\top \exp(\alpha_{0S}^{(k+1)} + \mathbf{X}_i^\top \boldsymbol{\beta}_1^{(k+1)} + \mathbf{X}_z^\top \boldsymbol{\beta}_2^{(k)})$$
$$\sum_{j\in I(t,z,\xi(z))} n_j \exp(\alpha_{0T}^{(k)} + \mathbf{W}_j^\top \boldsymbol{\beta}_3^{(k)}) d_{ij}^{-\delta^{(k)}} \frac{1}{L}\sum_{l=1}^{L}\left[\frac{(1-P_{izt})}{P_{izt}}\exp(u_{zl})\middle|\mathbf{y}_o, \boldsymbol{\Theta}^{(k)}\right]$$
$$-N_i^2 \mathbf{X}_z\mathbf{X}_z^\top \exp(2\alpha_{0S}^{(k+1)} + 2\mathbf{X}_i^\top \boldsymbol{\beta}_1^{(k+1)} + 2\mathbf{X}_z^\top \boldsymbol{\beta}_2^{(k)})\Big(\sum_{j\in I(t,z,\xi(z))} n_j \exp(\alpha_{0T}^{(k)} + \mathbf{W}_j^\top \boldsymbol{\beta}_3^{(k)}) d_{ij}^{-\delta^{(k)}}\Big)^2$$
$$\frac{1}{L}\sum_{l=1}^{L}\left[\frac{(1-P_{izt})}{P_{izt}^2}\exp(2u_{zl})\middle|\mathbf{y}_o, \boldsymbol{\beta}_3^{(k)}\right]\Bigg\}.$$

The following recursive equation is used for obtaining $\boldsymbol{\beta}_2$:

$$\boldsymbol{\beta}_2^{(k+1)} = \boldsymbol{\beta}_2^{(k)} - \frac{\frac{\partial}{\partial\boldsymbol{\beta}_2}\mathrm{E}\Big[\log L(\boldsymbol{\Theta};\mathbf{y}_c)|\mathbf{y}_o,\boldsymbol{\Theta}^{(k)}\Big]}{\frac{\partial^2}{\partial\boldsymbol{\beta}_2\partial\boldsymbol{\beta}_2^\top}\mathrm{E}\Big[\log L(\boldsymbol{\Theta};\mathbf{y}_c)|\mathbf{y}_o,\boldsymbol{\Theta}^{(k)}\Big]}.$$

4.2.4. CM-step 4

Let $\alpha_{0S} = \alpha_{0S}^{(k+1)}$, $\boldsymbol{\beta}_1 = \boldsymbol{\beta}_1^{(k+1)}$ and $\boldsymbol{\beta}_2 = \boldsymbol{\beta}_2^{(k+1)}$. We update $\alpha_{0T}^{(k)}$ by maximizing (5) over α_{0T}, with

$$\frac{\partial \mathrm{E}\Big[\log L(\boldsymbol{\Theta};\mathbf{y}_c)|\mathbf{y}_o,\boldsymbol{\Theta}\Big]}{\partial\alpha_{0T}} = -\sum_{t=1}^{T}\sum_{i\in S(t,z)}\sum_{z=1}^{m} I(Z_{it}=z) N_i \exp(\alpha_{0S}^{(k+1)} + \mathbf{X}_i^\top \boldsymbol{\beta}_1^{(k+1)} + \mathbf{X}_z^\top \boldsymbol{\beta}_2^{(k+1)})$$

$$\sum_{j\in I(t,z,\xi(z))} n_j \exp(\alpha_{0T}^{(k)} + \mathbf{W}_j^\top \boldsymbol{\beta}_3^{(k)}) d_{ij}^{-\delta^{(k)}} \frac{1}{L}\sum_{l=1}^{L}\left[\exp(u_{zl})\middle|\mathbf{y}_o, \boldsymbol{\Theta}^{(k)}\right]$$
$$+\sum_{t=1}^{T}\sum_{i\in E(t,z,\xi(z))\setminus E(t-1,z,\xi(z))}\sum_{z=1}^{m} I(Z_{it}=z)N_i \exp(\alpha_{0S}^{(k+1)} + \mathbf{X}_i^\top \boldsymbol{\beta}_1^{(k+1)} + \mathbf{X}_z^\top \boldsymbol{\beta}_2^{(k+1)})$$
$$\sum_{j\in I(t,z,\xi(z))} n_j \exp(\alpha_{0T}^{(k)} + \mathbf{W}_j^\top \boldsymbol{\beta}_3^{(k)}) d_{ij}^{-\delta^{(k)}} \frac{1}{L}\sum_{l=1}^{L}\left[\frac{(1-P_{izt})}{P_{izt}}\exp(u_{zl})\middle|\mathbf{y}_o, \boldsymbol{\Theta}^{(k)}\right],$$

and

$$\frac{\partial^2 \mathrm{E}\Big[\log L(\boldsymbol{\Theta};\mathbf{y}_c)|\mathbf{y}_o,\boldsymbol{\Theta}\Big]}{\partial \alpha_{0T}^2} = -\sum_{t=1}^{T}\sum_{i\in S(t,z)}\sum_{z=1}^{m} I(Z_{it}=z)N_i \exp(\alpha_{0S}^{(k+1)} + \mathbf{X}_i^\top \boldsymbol{\beta}_1^{(k+1)} + \mathbf{X}_z^\top \boldsymbol{\beta}_2^{(k+1)})$$
$$\sum_{j\in I(t,z,\xi(z))} n_j \exp(\alpha_{0T}^{(k)} + \mathbf{W}_j^\top \boldsymbol{\beta}_3^{(k)}) d_{ij}^{-\delta^{(k)}} \frac{1}{L}\sum_{l=1}^{L}\left[\exp(u_{zl})\middle|\mathbf{y}_o, \boldsymbol{\Theta}^{(k)}\right]$$
$$+\sum_{t=1}^{T}\sum_{i\in E(t,z,\xi(z))\setminus E(t-1,z,\xi(z))}\sum_{z=1}^{m} I(Z_{it}=z)\Bigg\{N_i \exp(\alpha_{0S}^{(k+1)} + \mathbf{X}_i^\top \boldsymbol{\beta}_1^{(k+1)} + \mathbf{X}_z^\top \boldsymbol{\beta}_2^{(k+1)})$$
$$\sum_{j\in I(t,z,\xi(z))} n_j \exp(\alpha_{0T}^{(k)} + \mathbf{W}_j^\top \boldsymbol{\beta}_3^{(k)}) d_{ij}^{-\delta^{(k)}} \frac{1}{L}\sum_{l=1}^{L}\left[\frac{(1-P_{izt})}{P_{izt}}\exp(u_{zl})\middle|\mathbf{y}_o, \boldsymbol{\Theta}^{(k)}\right]$$
$$-N_i^2 \exp(2\alpha_{0S}^{(k+1)} + 2\mathbf{X}_i^\top \boldsymbol{\beta}_1^{(k+1)} + 2\mathbf{X}_z^\top \boldsymbol{\beta}_2^{(k+1)})\Big(\sum_{j\in I(t,z,\xi(z))} n_j \exp(\alpha_{0T}^{(k)} + \mathbf{W}_j^\top \boldsymbol{\beta}_3^{(k)}) d_{ij}^{-\delta^{(k)}}\Big)^2$$
$$\frac{1}{L}\sum_{l=1}^{L}\left[\frac{(1-P_{izt})}{P_{izt}^2}\exp(2u_{zl})\middle|\mathbf{y}_o, \boldsymbol{\Theta}^{(k)}\right]\Bigg\}.$$

The following recursive equation (first-order Taylor expansion) is used for obtaining α_{0T}:

$$\alpha_{0T}^{(k+1)} = \alpha_{0T}^{(k)} - \frac{\frac{\partial}{\partial \alpha_{0T}}\mathrm{E}\Big[\log L(\boldsymbol{\Theta};\mathbf{y}_c)|\mathbf{y}_o,\boldsymbol{\Theta}^{(k)}\Big]}{\frac{\partial^2}{\partial \alpha_{0T}^2}\mathrm{E}\Big[\log L(\boldsymbol{\Theta};\mathbf{y}_c)|\mathbf{y}_o,\boldsymbol{\Theta}^{(k)}\Big]}.$$

4.2.5. CM-step 5

Let $\alpha_{0S} = \alpha_{0S}^{(k+1)}$, $\alpha_{0T} = \alpha_{0T}^{(k+1)}$, $\boldsymbol{\beta}_1 = \boldsymbol{\beta}_1^{(k+1)}$ and $\boldsymbol{\beta}_2 = \boldsymbol{\beta}_2^{(k+1)}$. We update $\boldsymbol{\beta}_3^{(k)}$ by maximizing (5) over $\boldsymbol{\beta}_3$, via

$$\frac{\partial \mathrm{E}\Big[\log L(\boldsymbol{\Theta};\mathbf{y}_c)|\mathbf{y}_o,\boldsymbol{\Theta}\Big]}{\partial \boldsymbol{\beta}_3} = -\sum_{t=1}^{T}\sum_{i\in S(t,z)}\sum_{z=1}^{m} I(Z_{it}=z)N_i \exp(\alpha_{0S}^{(k+1)} + \mathbf{X}_i^\top \boldsymbol{\beta}_1^{(k)} + \mathbf{X}_z^\top \boldsymbol{\beta}_2^{(k+1)})$$

$$\sum_{j\in I(t,z,\xi(z))} n_j \mathbf{W}_j \exp(\alpha_{0T}^{(k+1)} + \mathbf{W}_j^\top \boldsymbol{\beta}_3^{(k)}) d_{ij}^{-\delta^{(k)}} \frac{1}{L}\sum_{l=1}^{L}\left[\exp(u_{zl})\middle|\mathbf{y}_o, \boldsymbol{\Theta}^{(k)}\right]$$
$$+\sum_{t=1}^{T}\sum_{i\in E(t,z,\xi(z))\setminus E(t-1,z,\xi(z))}\sum_{z=1}^{m} I(Z_{it}=z) N_i \exp(\alpha_{0S}^{(k+1)} + \mathbf{X}_i^\top \boldsymbol{\beta}_1^{(k+1)} + \mathbf{X}_z^\top \boldsymbol{\beta}_2^{(k+1)})$$
$$\sum_{j\in I(t,z,\xi(z))} n_j \mathbf{W}_j \exp(\alpha_{0T}^{(k+1)} + \mathbf{W}_j^\top \boldsymbol{\beta}_3^{(k)}) d_{ij}^{-\delta^{(k)}} \frac{1}{L}\sum_{l=1}^{L}\left[\frac{(1-P_{izt})}{P_{izt}}\exp(u_{zl})\middle|\mathbf{y}_o, \boldsymbol{\Theta}^{(k)}\right],$$

and

$$\frac{\partial^2 \mathrm{E}\Big[\log L(\boldsymbol{\Theta};\mathbf{y}_c)|\mathbf{y}_o,\boldsymbol{\Theta}\Big]}{\partial\boldsymbol{\beta}_3\partial\boldsymbol{\beta}_3^\top} = -\sum_{t=1}^{T}\sum_{i\in S(t,z)}\sum_{z=1}^{m} I(Z_{it}=z) N_i \exp(\alpha_{0S}^{(k+1)} + \mathbf{X}_i^\top \boldsymbol{\beta}_1^{(k+1)} + \mathbf{X}_z^\top \boldsymbol{\beta}_2^{(k+1)})$$
$$\sum_{j\in I(t,z,\xi(z))} n_j \mathbf{W}_j \mathbf{W}_j^\top \exp(\alpha_{0T}^{(k+1)} + \mathbf{W}_j^\top \boldsymbol{\beta}_3^{(k)}) d_{ij}^{-\delta^{(k)}} \frac{1}{L}\sum_{l=1}^{L}\left[\exp(u_{zl})\middle|\mathbf{y}_o, \boldsymbol{\Theta}^{(k)}\right]$$
$$+\sum_{t=1}^{T}\sum_{i\in E(t,z,\xi(z))\setminus E(t-1,z,\xi(z))}\sum_{z=1}^{m} I(Z_{it}=z)\Bigg\{ N_i \exp(\alpha_{0S}^{(k+1)} + \mathbf{X}_i^\top \boldsymbol{\beta}_1^{(k+1)} + \mathbf{X}_z^\top \boldsymbol{\beta}_2^{(k+1)})$$
$$\sum_{j\in I(t,z,\xi(z))} n_j \mathbf{W}_j \mathbf{W}_j^\top \exp(\alpha_{0T}^{(k+1)} + \mathbf{W}_j^\top \boldsymbol{\beta}_3^{(k)}) d_{ij}^{-\delta^{(k)}} \frac{1}{L}\sum_{l=1}^{L}\left[\frac{(1-P_{izt})}{P_{izt}}\exp(u_{zl})\middle|\mathbf{y}_o, \boldsymbol{\Theta}^{(k)}\right]$$
$$-N_i^2 \exp(2\alpha_{0S}^{(k+1)} + 2\mathbf{X}_i^\top \boldsymbol{\beta}_1^{(k+1)} + 2\mathbf{X}_z^\top \boldsymbol{\beta}_2^{(k+1)})$$
$$\Big(\sum_{j\in I(t,z,\xi(z))} n_j \mathbf{W}_j \exp(\alpha_{0T}^{(k+1)} + \mathbf{W}_j^\top \boldsymbol{\beta}_3^{(k)}) d_{ij}^{-\delta^{(k)}}\Big)\Big(\sum_{j\in I(t,z,\xi(z))} n_j \mathbf{W}_j \exp(\alpha_{0T}^{(k+1)} + \mathbf{W}_j^\top \boldsymbol{\beta}_3^{(k)}) d_{ij}^{-\delta^{(k)}}\Big)^\top$$
$$\frac{1}{L}\sum_{l=1}^{L}\left[\frac{(1-P_{izt})}{P_{izt}^2}\exp(2u_{zl})\middle|\mathbf{y}_o, \boldsymbol{\Theta}^{(k)}\right]\Bigg\}.$$

The following recursive equation is used for obtaining $\boldsymbol{\beta}_3$:

$$\boldsymbol{\beta}_3^{(k+1)} = \boldsymbol{\beta}_3^{(k+1)} - \frac{\frac{\partial}{\partial\boldsymbol{\beta}_3}\mathrm{E}\Big[\log L(\boldsymbol{\Theta};\mathbf{y}_c)|\mathbf{y}_o,\boldsymbol{\Theta}^{(k)}\Big]}{\frac{\partial^2}{\partial\boldsymbol{\beta}_3\partial\boldsymbol{\beta}_3^\top}\mathrm{E}\Big[\log L(\boldsymbol{\Theta};\mathbf{y}_c)|\mathbf{y}_o,\boldsymbol{\Theta}^{(k)}\Big]}.$$

4.2.6. CM-step 6

Let $\alpha_{0S} = \alpha_{0S}^{(k+1)}$, $\alpha_{0T} = \alpha_{0T}^{(k+1)}$, $\boldsymbol{\beta}_1 = \boldsymbol{\beta}_1^{(k+1)}$, $\boldsymbol{\beta}_2 = \boldsymbol{\beta}_2^{(k+1)}$ and $\boldsymbol{\beta}_3 = \boldsymbol{\beta}_3^{(k+1)}$. We update $\delta^{(k)}$ by maximizing (5) over δ, via

$$\frac{\partial \mathrm{E}\Big[\log L(\boldsymbol{\Theta};\mathbf{y}_c)|\mathbf{y}_o,\boldsymbol{\Theta}\Big]}{\partial\delta} = \sum_{t=1}^{T}\sum_{i\in S(t,z)}\sum_{z=1}^{m} I(Z_{it}=z) N_i \exp(\alpha_{0S}^{(k+1)} + \mathbf{X}_i^\top \boldsymbol{\beta}_1^{(k+1)} + \mathbf{X}_z^\top \boldsymbol{\beta}_2^{(k+1)})$$

$$\sum_{j\in I(t,z,\xi(z))} n_j \exp(\alpha_{0T}^{(k+1)} + \mathbf{W}_j^\top \boldsymbol{\beta}_3^{(k+1)}) \ln(d_{ij}) d_{ij}^{-\delta^{(k)}} E\left[\exp(u_{zl}) \middle| \mathbf{y}_o, \boldsymbol{\Theta}^{(k)} \right]$$

$$-\sum_{t=1}^{T} \sum_{i\in E(t,z,\xi(z))\setminus E(t-1,z,\xi(z))} \sum_{z=1}^{m} I(Z_{it}=z) N_i \exp(\alpha_{0S}^{(k+1)} + \mathbf{X}_i^\top \boldsymbol{\beta}_1^{(k+1)} + \mathbf{X}_z^\top \boldsymbol{\beta}_2^{(k+1)})$$

$$\sum_{j\in I(t,z,\xi(z))} n_j \exp(\alpha_{0T}^{(k+1)} + \mathbf{W}_j^\top \boldsymbol{\beta}_3^{(k+1)}) \ln(d_{ij}) d_{ij}^{-\delta^{(k)}} \frac{1}{L} \sum_{l=1}^{L} \left[\frac{(1-P_{izt})}{P_{izt}} \exp(u_{zl}) \middle| \mathbf{y}_o, \boldsymbol{\Theta}^{(k)} \right],$$

and

$$\frac{\partial^2 \mathrm{E}\Big[\log L(\boldsymbol{\Theta}; \mathbf{y}_c) | \mathbf{y}_o, \boldsymbol{\Theta} \Big]}{\partial \delta^2} = -\sum_{t=1}^{T} \sum_{i\in S(t,z)} \sum_{z=1}^{m} I(Z_{it}=z) N_i \exp(\alpha_{0S}^{(k+1)} + \mathbf{X}_i^\top \boldsymbol{\beta}_1^{(k+1)} + \mathbf{X}_z^\top \boldsymbol{\beta}_2^{(k+1)})$$

$$\sum_{j\in I(t,z,\xi(z))} n_j \exp(\alpha_{0T}^{(k+1)} + \mathbf{W}_j^\top \boldsymbol{\beta}_3^{(k+1)}) (\ln(d_{ij}))^2 d_{ij}^{-\delta^{(k)}} \frac{1}{L} \sum_{l=1}^{L} \left[\exp(u_{zl}) \middle| \mathbf{y}_o, \boldsymbol{\Theta}^{(k)} \right]$$

$$+\sum_{t=1}^{T} \sum_{i\in E(t,z,\xi(z))\setminus E(t-1,z,\xi(z))} \sum_{z=1}^{m} I(Z_{it}=z) \Bigg\{ N_i \exp(\alpha_{0S}^{(k+1)} + \mathbf{X}_i^\top \boldsymbol{\beta}_1^{(k+1)} + \mathbf{X}_z^\top \boldsymbol{\beta}_2^{(k+1)})$$

$$\sum_{j\in I(t,z,\xi(z))} n_j \exp(\alpha_{0T}^{(k+1)} + \mathbf{W}_j^\top \boldsymbol{\beta}_3^{(k+1)}) (\ln(d_{ij}))^2 d_{ij}^{-\delta^{(k)}} \frac{1}{L} \sum_{l=1}^{L} \left[\frac{(1-P_{izt})}{P_{izt}} \exp(u_{zl}) \middle| \mathbf{y}_o, \boldsymbol{\Theta}^{(k)} \right]$$

$$-N_i^2 \exp(2\alpha_{0S}^{(k+1)} + 2\mathbf{X}_i^\top \boldsymbol{\beta}_1^{(k+1)} + 2\mathbf{X}_z^\top \boldsymbol{\beta}_2^{(k+1)}) \Big(\sum_{j\in I(t,z,\xi(z))} n_j \exp(\alpha_{0T}^{(k+1)} + \mathbf{W}_j^\top \boldsymbol{\beta}_3^{(k+1)}) \ln(d_{ij}) d_{ij}^{-\delta^{(k)}} \Big)^2$$

$$\frac{1}{L} \sum_{l=1}^{L} \left[\frac{(1-P_{izt})}{P_{izt}^2} \exp(2u_{zl}) \middle| \mathbf{y}_o, \boldsymbol{\beta}_3^{(k+1)} \right] \Bigg\}.$$

Hence, we have the following recursive equation for obtaining δ:

$$\delta^{(k+1)} = \delta^{(k)} - \frac{\frac{\partial}{\partial \delta} \mathrm{E}\Big[\log L(\boldsymbol{\Theta}; \mathbf{y}_c) | \mathbf{y}_o, \boldsymbol{\Theta}^{(k)} \Big]}{\frac{\partial^2}{\partial \delta^2} \mathrm{E}\Big[\log L(\boldsymbol{\Theta}; \mathbf{y}_c) | \mathbf{y}_o, \boldsymbol{\Theta}^{(k)} \Big]}.$$

4.2.7. CM-step 7

To update τ and λ on the M-step of the $(k+1)$th iteration, the following equation is be maximized:

$$\mathrm{E}\Big[\log(f(\mathbf{u})) \Big| \mathbf{y}_o, \boldsymbol{\Theta}^{(k)} \Big] = -\frac{m}{2} \ln(2\pi) + \frac{m}{2} \ln(\tau^2) + \frac{1}{2} \ln \left(\det \Big(\lambda \mathbf{D} + (1-\lambda) \mathbf{I} \Big) \right)$$

$$- \quad \frac{\tau^2}{2}\frac{1}{L}\sum_{l=1}^{L}\left[\mathbf{u}_l^T\Big(\lambda\mathbf{D}+(1-\lambda)\mathbf{I}\Big)\mathbf{u}_l\Big|\mathbf{y}_o,\boldsymbol{\Theta}^{(k)}\right].$$

Hence, τ and λ are obtained by a Newton-Raphson iterative procedure as follows:

$$\begin{pmatrix}\tau\\ \lambda\end{pmatrix}^{new} = \begin{pmatrix}\tau\\ \lambda\end{pmatrix}^{old} + B^{-1}A,$$

where A and B are the score vector and the expected information matrix whose elements can be defined as follows:

$$A(\tau) = \frac{\partial \mathrm{E}\Big[\log(f(\mathbf{u}))\Big|\mathbf{y}_o,\boldsymbol{\beta}_3\Big]}{\partial\tau} = \frac{m}{\tau} - \tau\frac{1}{L}\sum_{l=1}^{L}\left[\mathbf{u}_l^\top\Big(\lambda\mathbf{D}+(1-\lambda)\mathbf{I}\Big)\mathbf{u}_l\Big|\mathbf{y}_o,\boldsymbol{\Theta}^{(k)}\right],$$

$$A(\lambda) = \frac{\partial \mathrm{E}\Big[\log(f(\mathbf{u}))\Big|\mathbf{y}_o,\boldsymbol{\beta}_3\Big]}{\partial\lambda} = \frac{1}{2}tr\left(\Big(\lambda\mathbf{D}+(1-\lambda)\mathbf{I}\Big)^{-1}\Big(\mathbf{D}-\mathbf{I}\Big)\right) - \frac{\tau^2}{2}\frac{1}{L}\sum_{l=1}^{L}\left[\mathbf{u}_l^\top\Big(\mathbf{D}-\mathbf{I}\Big)\mathbf{u}_l\Big|\mathbf{y}_o,\boldsymbol{\Theta}^{(k)}\right],$$

$$B(\tau,\tau) = -\frac{\partial^2 \mathrm{E}\Big[\log(f(\mathbf{u}))\Big|\mathbf{y}_o,\boldsymbol{\beta}_3\Big]}{(\partial\tau)^2} = \frac{m}{\tau^2} + \frac{1}{L}\sum_{l=1}^{L}\left[\mathbf{u}_l^\top\Big(\lambda\mathbf{D}+(1-\lambda)\mathbf{I}\Big)\mathbf{u}_l\Big|\mathbf{y}_o,\boldsymbol{\Theta}^{(k)}\right],$$

$$B(\tau,\lambda) = -\frac{\partial^2 \mathrm{E}\Big[\log(f(\mathbf{u}))\Big|\mathbf{y}_o,\boldsymbol{\beta}_3\Big]}{\partial\tau\partial\lambda} = \tau\frac{1}{L}\sum_{l=1}^{L}\left[\mathbf{u}_l^\top\Big(\mathbf{D}-\mathbf{I}\Big)\mathbf{u}_l\Big|\mathbf{y}_o,\boldsymbol{\Theta}^{(k)}\right],$$

$$B(\lambda,\lambda) = -\frac{\partial^2 \mathrm{E}\Big[\log(f(\mathbf{u}))\Big|\mathbf{y}_o,\boldsymbol{\beta}_3\Big]}{(\partial\lambda)^2} = \frac{1}{2}tr\left(\Big(\mathbf{D}-\mathbf{I}\Big)\Big(\lambda\mathbf{D}+(1-\lambda)\mathbf{I}\Big)^{-1}\Big(\mathbf{D}-\mathbf{I}\Big)\Big(\lambda\mathbf{D}+(1-\lambda)\mathbf{I}\Big)^{-1}\right).$$

Using CM-step 1 to CM-step 7, we get updated model parameters at iteration $(k+1)$, and we continue this procedure until all model parameters converge.

5. Estimation of Model Parameter Standard Errors

Many methods have been suggested for the computation of model parameter standard errors estimate in the ECM context. Among these, the one best suited to be adapted for the MCECM is a method introduced by Louis (1982). In this approach, an estimate of the covariance matrix of the MLE $\hat{\boldsymbol{\Theta}}$ can be calculated via the inverse of the observed information matrix $I_{obs}(\hat{\Theta};\mathbf{y}_o)$. The formula for the observed information matrix is given by

$$I_{obs}(\hat{\Theta};\mathbf{y}_o) = I_{com}(\hat{\Theta};\mathbf{y}_o) - I_{miss}(\hat{\Theta};\mathbf{y}_o),$$

where the complete information matrix, $\mathrm{I}_{com}(\Theta;\mathbf{y}_o)$, and missing information matrix, $I_{miss}(\Theta;\mathbf{y}_o)$, can be approximated by

$$\mathrm{I}_{com}(\Theta;\mathbf{y}_o) \quad = \quad -\mathrm{E}\Big[\frac{\partial^2}{\partial\boldsymbol{\Theta}\partial\boldsymbol{\Theta}^\top}\log L(\boldsymbol{\Theta};\mathbf{y}_c)\Big|\mathbf{y}_o,\Theta\Big]$$

$$= -\frac{1}{L}\sum_{l=1}^{L}\frac{\partial^2}{\partial\boldsymbol{\Theta}\partial\boldsymbol{\Theta}^\top}\log L(\boldsymbol{\Theta};\mathbf{y}_c^l),$$

$$\begin{aligned} I_{miss}(\Theta;\mathbf{y}_o) &= \mathrm{E}\Big[\frac{\partial}{\partial\boldsymbol{\Theta}}\log L(\boldsymbol{\Theta};\mathbf{y}_c)\frac{\partial}{\partial\boldsymbol{\Theta}^\top}\log L(\boldsymbol{\Theta};\mathbf{y}_c)\Big|\mathbf{y}_o,\Theta\Big] - \mathrm{E}\Big[\frac{\partial}{\partial\boldsymbol{\Theta}}\log L(\boldsymbol{\Theta};\mathbf{y}_c)\Big|\mathbf{y}_o,\Theta\Big]\mathrm{E}\Big[\frac{\partial}{\partial\boldsymbol{\Theta}^\top}\log L(\boldsymbol{\Theta};\mathbf{y}_c)\Big|\mathbf{y}_o,\Theta\Big] \\ &= \frac{1}{L}\sum_{l=1}^{L}\frac{\partial}{\partial\boldsymbol{\Theta}}\log L(\boldsymbol{\Theta};\mathbf{y}_c^l)\frac{\partial}{\partial\boldsymbol{\Theta}^\top}\log L(\boldsymbol{\Theta};\mathbf{y}_c^l) - \left(\frac{1}{L}\sum_{l=1}^{L}\frac{\partial}{\partial\boldsymbol{\Theta}}\log L(\boldsymbol{\Theta};\mathbf{y}_c^l)\right)\times\left(\frac{1}{L}\sum_{l=1}^{L}\frac{\partial}{\partial\boldsymbol{\Theta}^\top}\log L(\boldsymbol{\Theta};\mathbf{y}_c^l)\right) \end{aligned}$$

where $\mathbf{y}_c^l = (\mathbf{y},\mathbf{z},\mathbf{u}_l)$ in which $\mathbf{u}_l$, $l = 1,\ldots,L$, are generated from the missing data distribution using the MCECM estimate of $\boldsymbol{\Theta}$. Since $\left(\frac{1}{L}\sum_{l=1}^{L}\frac{\partial}{\partial\boldsymbol{\Theta}}\log L(\boldsymbol{\Theta};\mathbf{y}_c^l)\right)\Big|_{\boldsymbol{\Theta}=\hat{\boldsymbol{\Theta}}} = 0$, we ultimately have

$$I_{obs}(\hat{\Theta};\mathbf{y}_o) = -\frac{1}{L}\sum_{l=1}^{L}\frac{\partial^2}{\partial\boldsymbol{\Theta}\partial\boldsymbol{\Theta}'}\log L(\boldsymbol{\Theta};\mathbf{y}_c^l) - \frac{1}{L}\sum_{l=1}^{L}\frac{\partial}{\partial\boldsymbol{\Theta}}\log L(\boldsymbol{\Theta};\mathbf{y}_c^l)\frac{\partial}{\partial\boldsymbol{\Theta}^\top}\log L(\boldsymbol{\Theta};\mathbf{y}_c^l).$$

6. Data analysis: COVID-19 across Manitoba

In this study, we analyze the second wave of COVID-19 across Manitoba and its five health regions (Interlake, Northern, Prairie, Southern and Winnipeg) from October 1, 2020 to January 31, 2021 (123 time points). Data were collected by Manitoba Health which include age at diagnosis, gender, date of diagnosis, and postal code of residence. Manitoba is divided into 96 LGAs and 2183 dissemination areas (DAs). The 6-character postal code is used to geocode the COVID-19 patients to one of the LGAs of Manitoba. Although in previous work DAs have been used as the individual units, here we use postal code regions (PCRs) as the individual units in order to achive modelling at a higher resolution.

As seen in the model defined in (1), we wish to consider the number of persons in each PCR as a risk factor for COVID-19 spread. As the population size of each DA is available in the 2016 Census dataset, and also the number of postal codes in each DA recorded in the Postal Code Conversion File (PCCF), the average population size of each postal code can be approximated by linking the 2016 Census and PCCF. The first three columns of Table 3 show that Manitoba contains 27,897 postal codes and during the second wave, 27,727 persons were infected which belong to a total of 7,045 postal codes. This information implies that in the infected PCRs we typically have more than one infected person. We extract these values from the dataset and use them in our proposed model as n_j for jth infected postal code region. Note also, within our SEIR framework, each PCR can be infected once and only once. We use the average diagnosis time of infected individuals in each PCR to define its exposure time.

Table 2: Number of local geographical area (LGA), number of infected individuals, number of postal codes and number of infected postal codes in Manitoba and also its five health regions.

Regions	# LGA	# Infected	# Postal codes	# Infected postal codes
Interlake	15	2211	1363	266
Northern	16	4044	1050	247
Southern	23	4239	2509	803
Prairie	17	1523	3079	412
Winnipeg	25	15710	19896	5317
Manitoba	96	27727	27897	7045

For each infected individual PCR, we use three individual-level covariates: "symptom rate", "proportion of males" and "proportion of population over 60 years". We divide patients into two groups: symptomatic and asymptomatic. The symptom rate is defined as the percentage of infected individuals in each PCR who have at least one COVID-19 symptom (e.g. fever, chills, cough and rash).

One of the main goals of this study is to assess the geographical variation of COVID-19 risk and its relationship with regional-level measure of socio-economic status (SES). We construct a measure of SES based upon on four census variables (income, unemployment, education and single parent) at LGA level. The SES factor scores are standardized factor scores derived using a principal component analysis of these four variables. This index variable measures socio-economic deprivation with higher SES values for a region indicating lower levels of SES. Figures 1 to 5 show the SES, number of postal codes, and incidence rate (the number of infected postal codes in each LGA divided by the total number of postal codes of the corresponding health region). As we can see from these figures, in all health regions except Northern, SES appears to be heavily associated with the incidence rate. Figure 2 also shows that not only do almost all Northern LGAs have a low level of SES, but also the more densely populated LGAs have more infected PCRs. Thus, we include SES as a regional-level covariate in each of our GD-ILM analyses, except for the analysis of the Northern health region.

Table 3 shows the estimates of parameters along with their standard errors (SEs) for GD-ILMs fitted to the COVID-19 dataset in the Northern, Interlake, Prairie, Southern and Winnipeg health regions. We show estimates based upon the latent and infectious periods estimated from the regions, and also based upon the complete Manitoba data analysis in Section 2 (Table 1). For the GD-ILMs fitted based on the health region-level periods, Table 3 shows that in Southern, Prairie and Winnipeg, people with higher SES (lower income) were more at risk of getting COVID-19. Although we have a negative value for SES in Interlake, this finding is confirmed through Figure 1(a) and (c). For the GD-ILMs fitted based on the Manitoba latent and infectious periods, in Prairie and Southern health regions, people with lower SES (higher income) were more at risk of getting COVID-19.

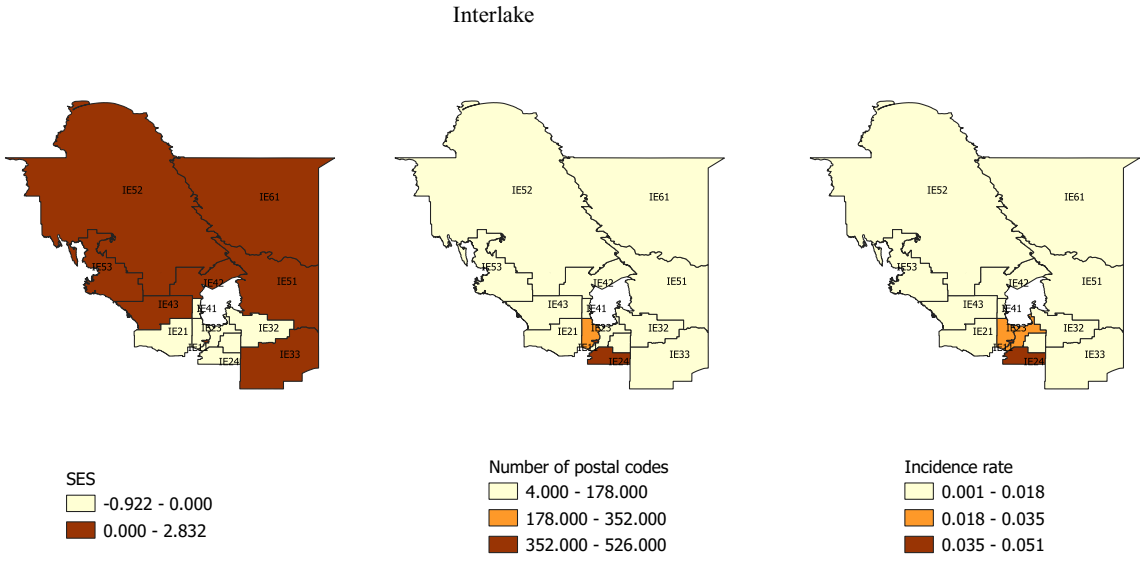

(a) (b) (c)

Figure 1: (a) SES, (b) number of postal code regions, and (c) incidence rates, in the Interlake health region.

Also, as we can see from Table 3, for both fitted models (based on both health region level and Manitoba latent and infectious periods), PCRs with higher rate of males and higher fraction of seniors were more vulnerable to COVID-19. Also, PCRs for all health regions except Prairie (when fitting our GD-ILM based on both Manitoba latent and infectious periods) with higher percentage of symptomatic persons were more at risk from COVID-19. It is worth mentioning that for the Winnipeg health region, the results of the both methods are very similar (Table 3) which are due to the fact that the majority of COVID-19 cases in Manitoba belongs to the Winnipeg health region. Moreover, for all health regions we observe that the estimated value of the spatial decay parameter (δ) is around 2.50 which indicates that the distance between PCRs was an important factor in the transmission of COVID-19. Also, for all health regions except Interlake, when fitting models using both health region-level latent and infectious periods, and for the model fitted on the COVID-19 data in Northen based on the Manitoba-wide periods, results show that spatial decay parameters are statistically significant, and we can conclude that for each health region, there is a spatial dependency between the LGAs. To assess which model has a better fit to the COVID-19 data, we use the Akaike information criterion (AIC; Akaike, 1974). The AIC is defined as AIC $= -2\, l(\hat{\boldsymbol{\Theta}}) + 2k^*$, where $l(\hat{\boldsymbol{\Theta}})$ is the maximum of log-likelihood and k^* is the number of model parameters. The model with smaller AIC is preferred. We can see from Table 3, that for all health regions the GD-ILMs with the regional-level estimated latent and infectious periods fit our data better based on the AIC. These result imply that

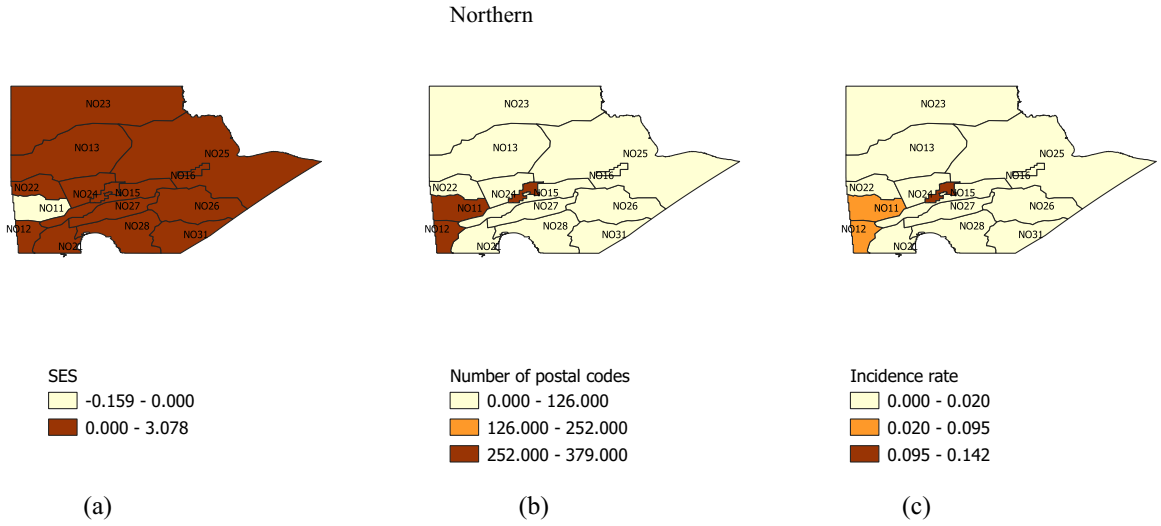

Figure 2: (a) SES, (b) number of postal code regions, and (c) incidence rates, in the Northern health region.

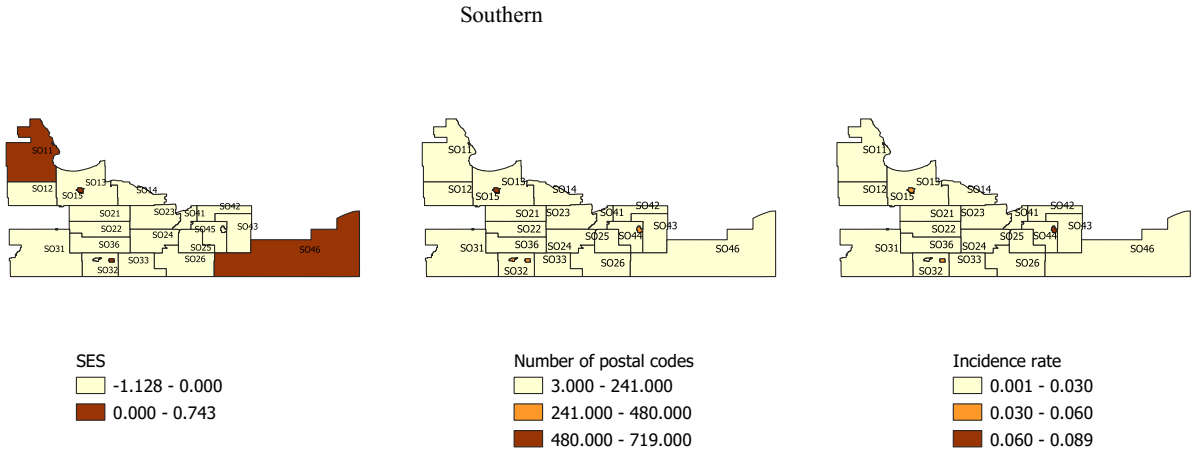

Figure 3: (a) SES, (b) number of postal code regions, and (c) incidence rates, in the Southern health region.

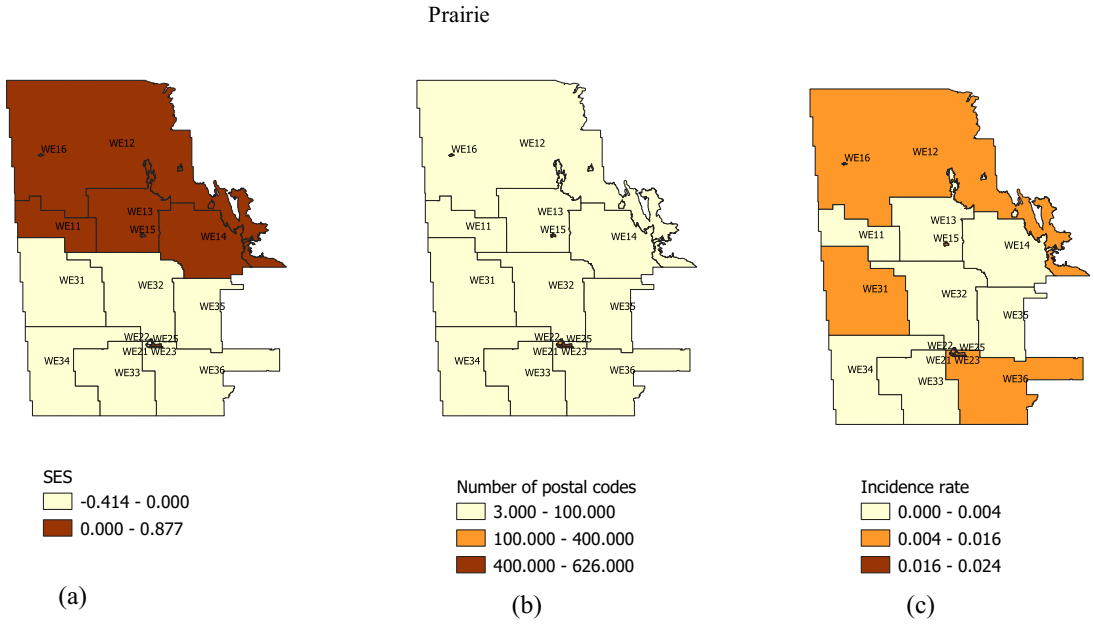

Figure 4: (a) SES, (b) number of postal code regions, and (c) incidence rates, in the Prairie health region.

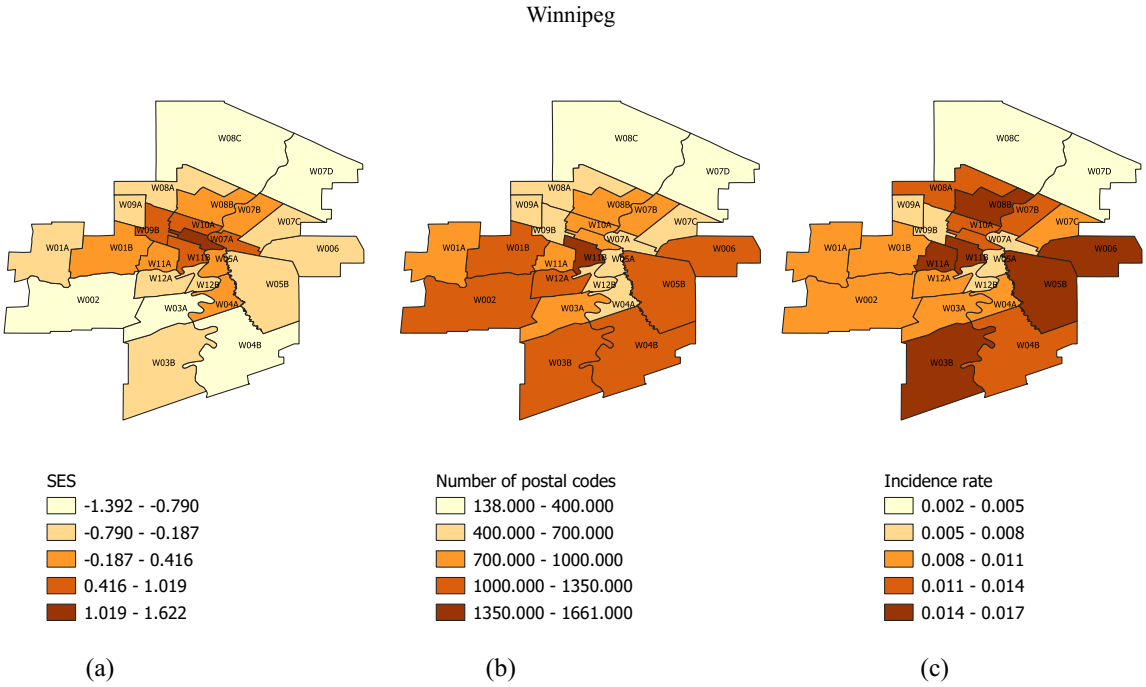

Figure 5: (a) SES, (b) number of postal code regions, and (c) incidence rates, in the Winnipeg health region.

Table 3: Model parameter estimates and their standard errors (S.E.) for the proposed GD-ILM based on Interlake, Prairie, Northern, Southern and Winnipeg actual incubation (λ_E) and infectious (λ_I) periods and Manitoba incubation and infectious periods; COVID-19 data across Manitoba, Canada, from October 1, 2020 to January 31, 2021.

		Actual periods		Manitoba periods	
		$\lambda_E = 3,\ \lambda_I = 5$		$\lambda_E = 3,\ \lambda_I = 6$	
Health region	Parameter	Est.	S.E.	Est.	S.E.
Interlake	α_{0S}	-3.000	$4.71e^{-5}$	-3.000	$3.41e^{-5}$
	SES	-2.167	$5.35e^{-5}$	-2.373	$5.38e^{-6}$
	α_{0T}	-3.000	$4.71e^{-5}$	-3.000	$3.41e^{-5}$
	Age 60+	1.551	$1.28e^{-4}$	1.557	$3.34e^{-5}$
	Symptom rate	0.458	$1.02e^{-4}$	0.462	$2.55e^{-5}$
	Male rate	1.512	$1.34e^{-4}$	1.503	$4.65e^{-5}$
	δ	2.495	$8.84e^{-6}$	2.495	$5.67e^{-6}$
	τ	1.014	0.281	0.954	0.179
	λ	0.381	0.379	0.797	0.247
	AIC	$2413.565e^{+3}$		$2504.250e^{+3}$	

		Actual periods		Manitoba periods	
		$\lambda_E = 2,\ \lambda_I = 6$		$\lambda_E = 3,\ \lambda_I = 6$	
Health region	Parameter	Est.	S.E.	Est.	S.E.
Southern	α_{0S}	-3.000	$3.18e^{-6}$	-2.000	$4.88e^{-7}$
	SES	0.277	$7.89e^{-6}$	-0.853	$9.68e^{-5}$
	α_{0T}	-3.000	$3.18e^{-6}$	-2.000	$4.88e^{-7}$
	Age 60+	1.940	$1.85e^{-6}$	1.976	$3.16e^{-7}$
	Symptom rate	0.019	$6.55e^{-6}$	1.013	$1.21e^{-6}$
	Male rate	1.944	$1.00e^{-5}$	1.962	$1.44e^{-6}$
	δ	2.541	$5.19e^{-7}$	2.695	$7.80e^{-8}$
	τ	0.847	0.126	0.852	0.125
	λ	0.960	0.055	0.886	0.143
	AIC	$2986.100\ e^{+3}$		$4132.340\ e^{+3}$	

		Actual periods		Manitoba periods	
		$\lambda_E = 9,\ \lambda_I = 5$		$\lambda_E = 3,\ \lambda_I = 6$	
Health region	Parameter	Est.	S.E.	Est.	S.E.
Prairie	α_{0S}	-3.000	$1.61e^{-5}$	-4.000	$1.92\ e^{-5}$
	SES	1.004	$4.28e^{-6}$	-0.274	$2.56\ e^{-6}$
	α_{0T}	-3.000	$1.61e^{-5}$	-4.000	$1.92\ e^{-5}$
	Age 60+	1.974	$5.64e^{-6}$	1.938	$2.36e^{-5}$
	Symptom rate	0.385	$4.01e^{-5}$	-0.445	$4.92e^{-5}$
	Male rate	1.439	$4.83e^{-5}$	1.155	$4.34e^{-5}$
	δ	2.555	$2.48e^{-6}$	2.404	$2.99e^{-6}$
	τ	0.659	0.113	0.619	0.106
	λ	0.916	0.114	0.939	0.084
	AIC	$9280.922e^{+3}$		$10246.820\ e^{+3}$	

		Actual periods		Manitoba periods	
		$\lambda_E = 4,\ \lambda_I = 5$		$\lambda_E = 3,\ \lambda_I = 6$	
Health region	Parameter	Est.	S.E.	Est.	S.E.
Winnipeg	α_{0S}	-2.000	$1.32e^{-7}$	-2.000	$1.32e^{-7}$
	SES	0.643	$4.45e^{-9}$	0.644	$4.43e^{-9}$
	α_{0T}	-2.000	$1.32e^{-7}$	-2.000	$1.32e^{-7}$
	Age 60+	1.755	$1.14e^{-7}$	1.756	$1.15e^{-7}$
	Symptom rate	1.216	$1.73e^{-7}$	1.215	$1.73e^{-7}$
	Male rate	1.585	$1.14e^{-7}$	1.585	$1.16e^{-7}$
	δ	2.686	$2.10e^{-8}$	2.686	$2.11e^{-8}$
	τ	0.727	0.109	0.727	0.109
	λ	0.830	0.207	0.830	0.207
	AIC	$3739.642\ e^{+3}$		$3739.754\ e^{+3}$	

		Actual periods		Manitoba periods	
		$\lambda_E = 1,\ \lambda_I = 7$		$\lambda_E = 3,\ \lambda_I = 6$	
Health region	Parameter	Est.	S.E.	Est.	S.E.
Northern	α_{0S}	-3.000	$1.51e^{-5}$	-3.000	$1.34e^{-5}$
	α_{0T}	-3.000	$1.51e^{-5}$	-3.000	$1.34e^{-5}$
	Age 60+	2.394	$3.67e^{-6}$	2.398	$4.46e^{-6}$
	Symptom rate	0.627	$4.45e^{-6}$	0.538	$1.91e^{-5}$
	Male rate	0.696	$1.69e^{-5}$	0.843	$1.74e^{-5}$
	δ	2.504	$2.69e^{-6}$	2.504	$2.38e^{-6}$
	τ	0.912	0.161	0.971	0.242
	λ	0.920	0.110	0.305	0.333
	AIC	$619.582e^{+3}$		$680.519e^{+3}$	

analyzing health regions separately give us more accurate results in comparison with the models fitted with latent and infectious periods from all of Manitoba.

In addition, for each health region, we predict the average infectivity rates using the estimated parameters under both sets of latent and infections periods. The average infectivity rates for LGAs of health regions over the entire time interval (123 time points) are displayed in Figures 6 to 10. It is evident from Figures 6 to 9 that the average infectivity rates of COVID-19 under the regional-level estimated latent and infectious periods are different from those based on the Manitoba-wide estimates. This will also imply that health region heterogeneity in the latent and infectious periods is important.

7. Simulation studies

Here, we consider simulation studies to evaluate the performance of our proposed approach. We consider PCRs as the individual-level units and generate epidemics through 960 PCRs located on a 8×8 grid with 64 geographical areas so there are 15 postal codes

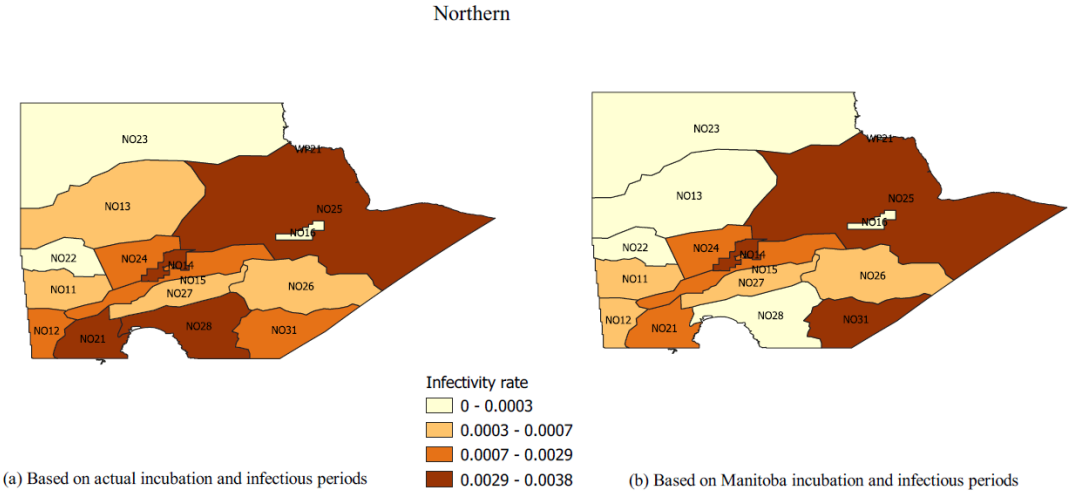

Figure 6: Average infectivity rate for Northern health region.

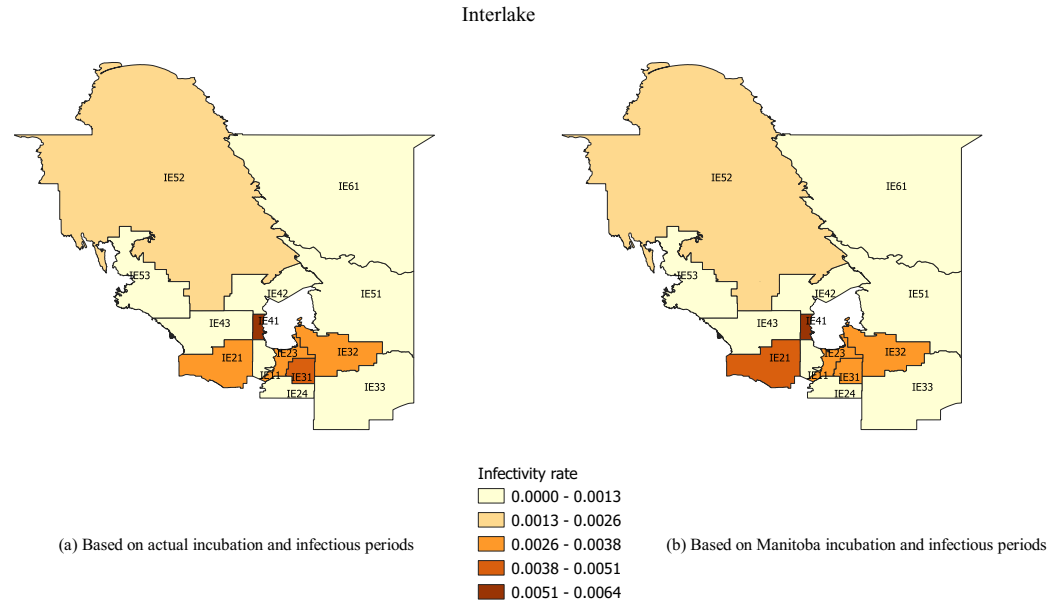

Figure 7: Average infectivity rate for the Interlake health region.

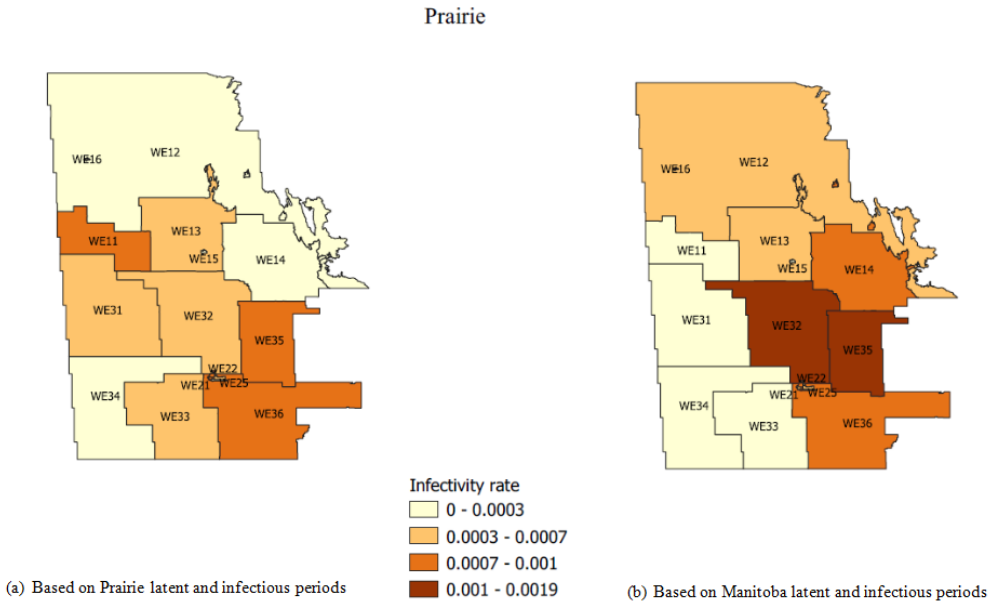

(a) Based on Prairie latent and infectious periods

(b) Based on Manitoba latent and infectious periods

Figure 8: Average infectivity rate for the Prairie health region.

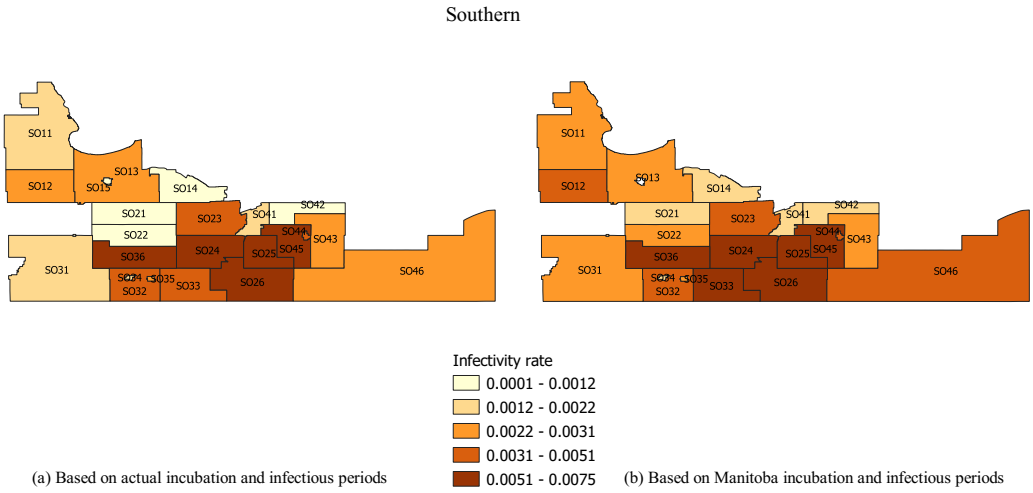

(a) Based on actual incubation and infectious periods

(b) Based on Manitoba incubation and infectious periods

Figure 9: Average infectivity rate for the Southern health region.

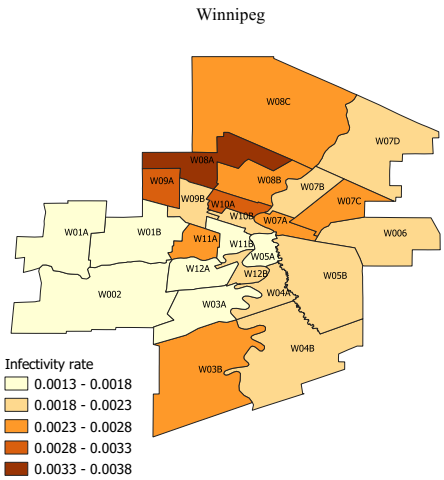

Figure 10: Average infectivity rate for the Winnipeg health region.

in each area. The latitude (x) and longitude (y) coordinates of the areas are given by all combinations (x, y) for $x, y = 3, 6, 9, \ldots, 24$. We generate the population size of each PCRs such that $N_i \sim$ Uniform(1,100) (i=1, ..., 960). Further, for each infected PCR j that has more than one resident, in order to determine its number of infectious individuals, namely $n_j \in Z$, we assume one of three percentages of residents infected, $\Pr \in \{0.10, 0.20, 0.30\}$, and $n_j = \Pr \times N_j$. We then generate two regional-level covariates X_{21} and X_{22} from $N(0, 1)$ and $U(0, 1)$, respectively, to incorporate in the susceptibility function. Individual-level covariates W_{31} and W_{32} are generated from $N(0, 1)$ and $U(0, 1)$, respectively, to embed in the transmissibility function. d_{ij} is calculated using an Euclidean distance between individuals i and j. For the spatial random effect parameters, we set the precision parameter to $\tau = 0.50$, and we consider two different values of the spatial dependence parameter, $\lambda \in \{0.50, 0.80\}$, with the aim of exploring the effect of different strengths of spatial correlation. Other values of model parameters used in the simulation study are given in Tables 5 and 6.

We simulated 250 random data sets from the GD-ILM on the 8×8 grid. To start an epidemic, one PCR is randomly exposed in each of the cells at $t = 1$. Epidemics are simulated over an epidemic length of $T = 35$ time units. In order to determine the latent period (λ_E) and infectious period (λ_I), we fit the homogeneous SEIR model to the generated data. Since our GD-ILM is a discrete time model, we use the rounded estimates of these periods.

Table 4: Rounded incubation period (λ_E) and infectious period (λ_I) of 8×8 grid and its sub-grids obtained from 100 SEIR model iteration.

Grids	λ_E	λ_I
5×5 grid	2	6
5×3 grid	3	5
3×8 grid	4	4
8×8 grid	2	5

Results shows that across the entire population $\lambda_E = 2$ and $\lambda_I = 5$. Then, we split the entire 8×8 grid into three parts consisting of grids of size 5×5, 5×3 and 3×8 grids. In order to determine the λ_E and λ_I of each sub-grid, we fit the homogeneous SEIR model to the corresponding sub-grid data. As we can see from Table 4, latent and infectious periods vary from one sub-grid to another sub-grid and they are entirely different from the whole 8×8 grid periods.

In the following, for each sub-grid, we provide simulation results based on 250 runs in terms of two different scenarios. In the first scenario results are obtained using latent and infectious periods estimated at the sub-grid level, and in the second scenario, latent and infectious periods estimated across the entire 8×8 grid. Further, we report results of the simulation study for the entire 8×8 grids based on its estimated latent and infectious periods. The model parameters are estimated via the MCECM algorithm. Tables 5 and 6 present the average of the estimated parameters for the regional-level covariates (β_{21}, β_{22}), individual-level covariates (β_{31}, β_{32}), spatial decay parameter (δ), and parameters in the spatial random effects $(\tau,\ \lambda)$ along with their estimated standard errors in the case of $\lambda = 0.5$ and 0.8, respectively. As it can be seen from these tables, in all three sub-grids, individual- and regional-level covariate coefficient estimations are generally unbiased in the case of sub-grid time periods. Although we have reasonable results for estimated parameters of 5×5 sub-grid based on entire 8×8 grid periods, results are less precise in compare with those obtained using sub-grid time periods. For the both 5×3 and 3×8 sub-grids, model parameter estimates are biased based on the 8×8 grid latent and infectious time periods. Finally, the last two columns of Tables 5 and 6 display unbiased estimate of parameters for entire 8×8 grid based on its time periods. In terms of spatial precision (τ) parameter we have a slightly over-estimation for sub-grids (5×5, 5×3 and 3×8) compared to the entire 8×8 grid . In the case of spatial dependency (λ) parameter, it is not surprising that for almost all percentage of infected individuals, we have more accurate estimation for sub-grids compared to the entire grid. Also, we have more accurate estimation for $\lambda = 0.50$ compared to $\lambda = 0.80$ in our specific set-up.

In the following, in order to determine the cells with higher infectivity rate, we obtain the infectivity rates of infectious disease over time at each area of sub-grids according

Table 5: True value of model parameters along with the average parameter estimates (Est.) and average standard errors of the estimated parameters (S.E.) over 250 simulation runs in the case of $\lambda = 0.5$.

			5×5 grid				5×3 grid				3×8 grid				8×8 grid	
			Actual periods		8×8 grid periods		Actual periods		8×8 grid periods		Actual periods		8×8 grid periods		Actual periods	
	Parameter	True	Est.	S.E.	Est.	S.E.	Est.	S.E.	Est.	S.E.	Est.	S.E.	Est.	S.E.	Est.	S.E.
	α_{0S}	0.00	0.084	0.062	0.211	0.070	0.238	0.102	0.485	0.123	0.166	0.079	0.401	0.119	0.034	0.041
	β_{21}	1.00	0.993	0.087	0.967	0.094	0.976	0.117	0.709	0.141	1.005	0.104	0.615	0.243	0.996	0.056
	β_{22}	1.00	0.998	0.110	0.952	0.125	1.011	0.219	0.909	0.274	1.023	0.164	0.201	0.424	0.992	0.078
	α_{0T}	0.00	-0.024	0.004	-0.061	0.006	-0.077	0.102	-0.578	0.019	-0.014	0.010	-0.770	0.009	-0.016	0.002
Pr = 0.10	β_{31}	1.00	1.004	0.151	0.978	0.155	0.979	0.218	0.816	0.259	1.005	0.139	1.014	0.305	0.992	0.091
	β_{32}	1.00	0.927	0.224	0.866	0.249	0.817	0.276	0.269	0.369	0.940	0.194	-0.102	0.385	0.962	0.122
	δ	2.50	2.514	0.014	2.529	0.016	2.536	0.023	2.691	0.033	2.515	0.019	2.764	0.040	2.508	0.009
	τ	0.50	0.551	0.103	0.555	0.106	0.562	0.129	0.535	0.133	0.555	0.104	0.520	0.088	0.525	0.069
	λ	0.50	0.493	0.279	0.492	0.284	0.507	0.135	0.667	0.291	0.454	0.272	0.636	0.240	0.460	0.204
	α_{0S}	0.00	0.148	0.056	0.183	0.060	0.208	0.088	0.267	0.104	0.353	0.059	0.048	0.096	0.059	0.036
	β_{21}	1.00	0.982	0.076	0.948	0.081	0.987	0.101	0.566	0.121	1.030	0.075	0.554	0.116	0.998	0.049
	β_{22}	1.00	1.005	0.100	0.960	0.107	1.010	0.175	1.105	0.233	1.117	0.123	0.182	0.215	1.010	0.068
	α_{0T}	0.00	-0.018	0.003	-0.046	0.006	-0.074	0.009	-0.650	0.007	0.018	0.007	-0.718	0.004	0.001	0.001
Pr = 0.20	β_{31}	1.00	0.979	0.110	0.974	0.148	0.983	0.206	0.865	0.289	1.012	0.099	1.009	0.230	1.010	0.077
	β_{32}	1.00	0.977	0.162	0.904	0.210	0.834	0.251	0.195	0.359	0.966	0.138	-0.154	0.285	0.963	0.107
	δ	2.50	2.512	0.012	2.522	0.013	2.535	0.202	2.694	0.031	2.510	0.013	2.750	0.027	2.504	0.008
	τ	0.50	0.544	0.099	0.557	0.104	0.579	0.129	0.554	0.116	0.557	0.104	0.535	0.095	0.537	0.072
	λ	0.50	0.508	0.269	0.509	0.277	0.504	0.116	0.667	0.303	0.465	0.279	0.639	0.254	0.406	0.199
	α_{0S}	0.00	0.106	0.054	0.178	0.058	0.230	0.081	0.510	0.120	0.334	0.056	0.152	0.082	0.139	0.033
	β_{21}	1.00	0.998	0.072	0.980	0.076	0.995	0.094	0.632	0.180	1.020	0.071	0.517	0.097	0.997	0.045
	β_{22}	1.00	1.016	0.097	0.962	0.104	1.015	0.156	0.661	0.332	1.119	0.116	0.099	0.188	1.013	0.065
	α_{0T}	0.00	0.005	0.002	-0.029	0.003	-0.058	0.009	-0.782	0.011	0.013	0.006	-0.781	0.004	0.005	0.001
Pr = 0.30	β_{31}	1.00	0.989	0.104	0.973	0.125	0.975	0.207	0.731	0.301	1.019	0.125	1.028	0.208	0.994	0.089
	β_{32}	1.00	0.992	0.155	0.943	0.181	0.872	0.237	0.085	0.332	0.947	0.165	-0.197	0.239	0.978	0.114
	δ	2.50	2.507	0.012	2.517	0.013	2.530	0.018	2.697	0.026	2.510	0.012	2.759	0.024	2.505	0.007
	τ	0.50	0.553	0.103	0.555	0.101	0.572	0.136	0.583	0.122	0.546	0.102	0.549	0.108	0.523	0.069
	λ	0.50	0.480	0.271	0.502	0.278	0.480	0.167	0.631	0.310	0.470	0.277	0.554	0.315	0.438	0.201

to (2). To save space, we only provide the infectivity rate figures for the model with Pr = 0.20 and $\delta = 2.50$, $\tau = 0.50$, and $\lambda = 0.50$. It is evident from Figure 11 that, for all sub-grids, the cells with higher infectivity rates are different between the model fitted based on sub-grids latent and infectious time periods and model fitted based on entire 8×8 grid latent and infectious time periods which confirm that using low resolution (entire grid time periods) may lead to wrong conclusions.

8. Conclusion

We proposed a SEIR GD-ILM that allows us to consider the spatio-temporal spread of COVID- 19 in a disjoint communities (rather than entire population) when individual level data are available. We carried out model parameter estimation via a MCECM algorithm and tested the accuracy of the proposed method through simulation studies.

Table 6: True value of model parameters along with the average parameter estimates (Est.) and average standard errors of the estimated parameters (S.E.) over 250 simulation runs in the case of $\lambda = 0.8$.

			5×5 grid				5×3 grid				3×8 grid				8×8 grid	
			Actual periods		8×8 grid periods		Actual periods		8×8 grid periods		Actual periods		8×8 grid periods		Actual periods	
	Parameter	True	Est.	S.E.	Est.	S.E.	Est.	S.E.	Est.	S.E.	Est.	S.E.	Est.	S.E.	Est.	S.E.
	α_{0S}	0.00	0.093	0.061	0.344	0.067	0.220	0.106	0.432	0.152	0.399	0.070	0.299	0.123	0.080	0.041
	β_{21}	1.00	0.994	0.087	0.963	0.096	0.986	0.132	0.723	0.150	1.014	0.092	0.723	0.179	1.003	0.056
	β_{22}	1.00	1.009	0.110	0.955	0.121	0.998	0.242	0.932	0.304	1.083	0.144	0.450	0.281	0.990	0.076
	α_{0T}	0.00	-0.010	0.006	-0.082	0.006	-0.061	0.021	-0.532	0.030	-0.004	0.007	-0.645	0.012	-0.009	0.011
Pr = 0.10	β_{31}	1.00	0.995	0.154	0.960	0.174	1.001	0.223	0.981	0.269	1.007	0.120	0.993	0.295	0.999	0.080
	β_{32}	1.00	0.955	0.231	0.841	0.256	0.827	0.290	0.217	0.405	0.936	0.167	0.009	0.321	0.954	0.111
	δ	2.50	2.511	0.014	2.539	0.015	2.534	0.025	2.657	0.037	2.516	0.016	2.713	0.037	2.509	0.009
	τ	0.50	0.561	0.092	0.559	0.091	0.596	0.118	0.572	0.107	0.561	0.092	0.592	0.090	0.529	0.058
	λ	0.80	0.683	0.227	0.746	0.232	0.668	0.264	0.778	0.233	0.674	0.229	0.712	0.183	0.692	0.182
	α_{0S}	0.00	0.098	0.057	0.192	0.061	0.240	0.086	0.286	0.122	0.397	0.060	0.673	0.074	0.071	0.037
	β_{21}	1.00	0.990	0.079	0.961	0.085	0.984	0.101	0.707	0.138	1.004	0.078	0.764	0.104	1.004	0.050
	β_{22}	1.00	1.017	0.103	0.961	0.108	1.034	0.173	0.820	0.223	1.089	0.126	0.091	0.169	0.987	0.072
	α_{0T}	0.00	-0.009	0.005	-0.043	0.005	-0.055	0.016	-0.568	0.019	0.010	0.007	-0.777	0.013	-0.011	0.007
Pr = 0.20	β_{31}	1.00	1.007	0.132	0.974	169	0.991	0.179	0.838	0.214	1.024	0.098	1.046	0.107	0.991	0.081
	β_{32}	1.00	0.946	0.193	0.911	0.236	0.865	0.226	0.341	0.372	0.950	0.142	-0.305	0.176	0.976	0.109
	δ	2.50	2.510	0.013	2.523	0.014	2.530	0.019	2.667	0.032	2.512	0.014	2.772	0.022	2.507	0.008
	τ	0.50	0.561	0.091	0.561	0.092	0.587	0.118	0.646	0.128	0.559	0.092	0.586	0.102	0.526	0.058
	λ	0.80	0.701	0.215	0.697	0.229	0.674	0.268	0.764	0.212	0.680	0.225	0.723	0.254	0.690	0.184
	α_{0S}	0.00	0.085	0.056	0.213	0.057	0.267	0.082	0.332	0.112	0.296	0.057	0.093	0.098	0.051	0.037
	β_{21}	1.00	0.984	0.075	0.968	0.074	0.992	0.095	0.632	0.140	1.016	0.073	0.288	0.242	1.007	0.049
	β_{22}	1.00	1.024	0.101	0.983	0.102	1.011	0.162	0.691	0.220	1.112	0.119	0.346	0.204	0.956	0.071
	α_{0T}	0.00	-0.009	0.003	-0.033	0.006	-0.056	0.007	-0.623	0.010	0.009	0.006	-0.764	0.012	-0.029	0.006
Pr = 0.30	β_{31}	1.00	1.003	0.108	0.982	0.179	0.978	0.177	0.912	0.308	1.005	0.107	0.897	0.338	1.001	0.081
	β_{32}	1.00	0.952	0.170	0.926	0.249	0.859	0.226	0.117	0.333	0.958	0.145	-0.102	0.284	0.939	0.107
	δ	2.50	2.509	0.012	2.520	0.012	2.530	0.018	2.679	0.034	2.509	0.013	2.774	0.029	2.511	0.008
	τ	0.50	0.558	0.092	0.579	0.097	0.590	0.123	0.653	0.130	0.570	0.093	0.581	0.101	0.521	0.056
	λ	0.80	0.682	0.224	0.668	0.228	0.660	0.273	0.676	0.250	0.682	0.229	0.704	0.236	0.704	0.177

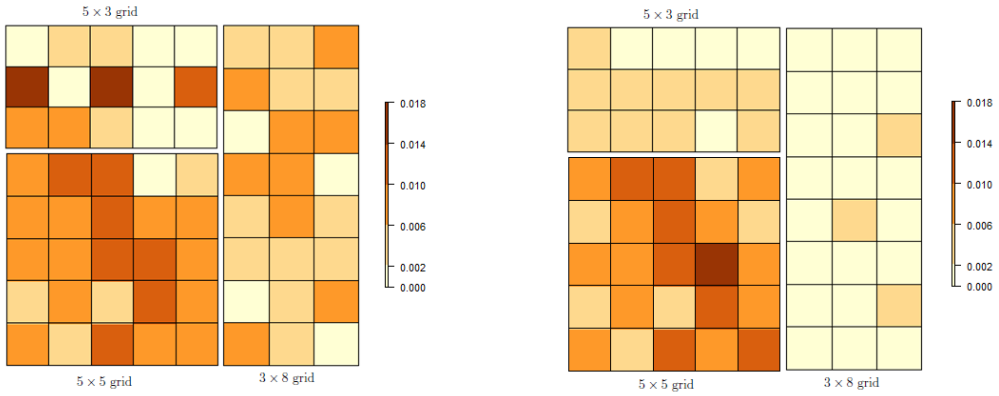

(a) Based on actual incubation and infectious periods

(b) Based on 8×8 grid incubation and infectious periods

Figure 11: Predicted average rate of infectivity based on (a) actual incubation and infectious time periods of sub-grids and (b) 8×8 grid incubation and infectious time periods.

Also, we applied this model to data from the second wave of COVID-19 in Manitoba. We considered the dynamics of COVID-19 transmission over all of Manitoba as well as its five health regions separately to ascertain the importance of accounting for health region level heterogeneity. In our data analysis, we used socio-economic status (SES) as regional-level covariate measured at the LGA level, and three covariates (symptom rate, proportion of males, and proportion of people over 60 years) as covariates measured at the postal-code level. We showed that latent and infectious time periods vary from one health region to another health region and they are different from the entire Manitoba latent and infectious time periods. For each health region, we fitted two models: (1) fitted with health region specific latent and infectious periods and (2) fitted with the entire Manitoba latent and infectious time periods. Further, for each health region, we selected the best fitted model using AIC. Finally, we showed how infectivity rate maps could be used to determine LGAs with higher average infectivity rates.

There are some topics may be of interest for future work. One can expand our proposed model to study SEIRS (susceptible-exposed-infected-removed- susceptible) frameworks that allow us to consider an infectious disease (e.g., COVID-19) with a different event history. Further, in our proposed approach, the infectious time period for each individual was assumed to be constant, and the removal time of individuals was known. These assumptions can be relaxed, considering removal times and infectious periods as unknown variables that need to be estimated. Further, in this study, we used a power-law distance kernel, but that can be replaced by alternative kernels such as an exponential distance kernel (see, for example, Chen et al., 2014).

Acknowledgments

Constructive comments and suggestions of a reviewer, which led to an improved version of this article, are greatly appreciated. This research was partially supported by Research Manitoba COVID-19 Rapid Response Grant.

References

Akaike, H. (1974). A new look at the statistical model identification. *IEEE Transactions on Automatic Control*, 19, 716–723.

Amiri, L., Torabi, M., Deardon, R. and Pickles, M. (2021). Spatial modeling of individual-level infectious disease transmission: tuberculosis data in Manitoba, Canada. *Statistics in Medicine,* 40(7), 1678-1704.

Anderson, R.M. and May, R.M. (1992). *Infectious diseases of humans: dynamics and control.* Oxford university press.

Balsa, C., Lopes, I., Guarda, T., and Rufino, J. (2021). Computational simulation of the COVID-19 epidemic with the SEIR stochastic model. *Computational and Mathematical Organization Theory,* 1-19.

ben Khedher, N., Kolsi, L., and Alsaif, H. (2021). A multi-stage SEIR model to predict the potential of a new COVID-19 wave in KSA after lifting all travel restrictions. *Alexandria Engineering Journal,* 60(4), 3965-3974.

Besag, J., York, J. and Mollié, A. (1991). Bayesian image restoration, with two applications in spatial statistics. *Annals of the institute of statistical mathematics,* 43(1), 1-20.

Chen, D., Moulin, B. and Wu, J. (2014). *Analyzing and modeling spatial and temporal dynamics of infectious diseases.* John Wiley & Sons, Hoboken, New Jersey.

Chen, Z.L., Zhang, Q., Lu, Y., Guo, Z.M., Zhang, X., Zhang, W.J., Guo, C., Liao, C.H., Li, Q.L., Han, X.H. and Lu, J.H. (2020). Distribution of the COVID-19 epidemic and correlation with population emigration from Wuhan, China. *Chinese medical journal,* 133(9), 1044-1050.

Cooper, I., Mondal, A., and Antonopoulos, C. G. (2020). A SIR model assumption for the spread of COVID-19 in different communities. *Chaos, Solitons & Fractals,* 139, 110057.

Daley, D., & Gani, J. (1999). *Epidemic Modeling: An Introduction.* New York: Cambridge University.

Deardon, R., Brooks, S. P., Grenfell, B. T., Keeling, M. J., Tildesley, M. J., Savill, N. J., et al. (2010). Inference for individual-level models of infectious diseases in large populations. *Statistica Sinica,* 20(1), 239-261.

Dempster, A. P., Laird, N. M. and Rubin, D. B. (1977). Maximum likelihood from incomplete data via the EM algorithm. *Journal of the Royal Statistical Society, Series B,* 39, 1-38 .

de Souza, C. D. F., Machado, M. F., and do Carmo, R. F. (2020). Human development, social vulnerability and COVID-19 in Brazil: A study of the social determinants of health. *Infectious Diseases of Poverty,*2020, 9, 1-10.

Ghostine, R., Gharamti, M., Hassrouny, S., and Hoteit, I. (2021). An extended seir model with vaccination for forecasting the covid-19 pandemic in saudi arabia using an ensemble kalman filter. *Mathematics,* 9(6), 636.

Giordano, G., Blanchini, F., Bruno, R., Colaneri, P., Di Filippo, A., Di Matteo, A., and Colaneri, M. (2020). Modelling the COVID-19 epidemic and implementation of population-wide interventions in Italy. *Nature medicine,* 26(6), 855-860.

Hartley, H. (1958). Maximum likelihood estimation from incomplete data. *Biometrics,* 14, 174-194.

He, X., Lau, E. H., Wu, P., Deng, X., Wang, J., Hao, X., Lau, Y. C., Wong, J. Y., Guan, Y., Tan, X. and Mo, X. (2020). Temporal dynamics in viral shedding and transmissibility of COVID-19. *Nature medicine,* 26(5), 672-675.

Kissler, S. M., Tedijanto, C., Goldstein, E., Grad, Y. H., and Lipsitch, M. (2020). Projecting the transmission dynamics of SARS-CoV-2 through the postpandemic period. *Science,* 368(6493), 860-868.

Leroux, B. G., Lei, X. and Breslow, N. (2000). Estimation of disease rates in small areas: a new mixed model for spatial dependence. In *Statistical models in epidemiology, the environment, and clinical trials* (pp. 179-191). Springer, New York, NY.

Louis, T. A. (1982). Finding the observed information matrix when using the EM algorithm. *Journal of the Royal Statistical Society, Series B,* 44, 226-233.

Macharia, P. M., Joseph, N. K., and Okiro, E. A. (2020). A vulnerability index for COVID-19: spatial analysis at the subnational level in Kenya. *BMJ global health,* 5(8), e003014.

Mahsin, M. D., Deardon, R. and Brown, P. (2020). Geographically dependent individual-level models for infectious diseases transmission. *Biostatistics*. DOI:10.1093/biostatistics/kxaa009.

Meng, X. L. and Rubin, D. B. (1993). Maximum likelihood estimation via the ECM algorithm: A general framework. *Biometrika,* 80(2), 267–278.

Ramírez, I. J., and Lee, J. (2020). COVID-19 emergence and social and health determinants in Colorado: a rapid spatial analysis. *International journal of environmental research and public health,* 17(11), 3856.

Santos, J. P. C. D., Siqueira, A. S. P., Praça, H. L. F., and Albuquerque, H. G. (2020). Vulnerability to severe forms of COVID-19: an intra-municipal analysis in the city of Rio de Janeiro, Brazil. *Cadernos de Saúde Pública,* 36, e00075720.

Tuite, A. R., Fisman, D. N., and Greer, A. L. (2020). Mathematical modelling of COVID-19 transmission and mitigation strategies in the population of Ontario, Canada. *CMAJ,* 192(19), E497-E505.

Wei, G. C. and Tanner, M. A. (1990). A Monte Carlo implementation of the EM algorithm and the poor man's data augmentation algorithms. *Journal of the American statistical Association,* 85(411), 699-704.

Xiong, Y., Wang, Y., Chen, F., and Zhu, M. (2020). Spatial statistics and influencing factors of the COVID-19 epidemic at both prefecture and county levels in Hubei Province, China. *International journal of environmental research and public health,* 17(11), 3903.

Zhang, C. H., and Schwartz, G. G. (2020). Spatial disparities in coronavirus incidence and mortality in the United States: an ecological analysis as of May 2020. *The Journal of Rural Health,* 36(3), 433-445.